PCCP

Isothermal Onsager matrices and acceptor size effect on mass/charge transport properties of $La_{1.9}A_{0.1}NiO_{3.95+\delta}$ (A=Ca,Sr)

Journal:	*Physical Chemistry Chemical Physics*
Manuscript ID:	CP-ART-12-2013-055228.R1
Article Type:	Paper
Date Submitted by the Author:	02-Mar-2014
Complete List of Authors:	Kim, Hong-Seok; Seoul National University, Materials Science and Engineering Yoo, Han-Ill; Seoul National University, School of Materials Science and Engineering

Isothermal Onsager matrices and acceptor size effect on mass/charge transport properties of $La_{1.9}A_{0.1}NiO_{3.95+\delta}$ (A=Ca,Sr)

Hong-Seok Kim and Han-Ill Yoo#

Department of Materials Science & Engineering,

Seoul National University, Seoul 151-744, Republic of Korea

Abstract

Isothermal Onsager transport coefficient matrices have been established experimentally for the systems of $La_{1.9}A_{0.1}NiO_{3.95+\delta}$ doped with different-size acceptors A=Ca^{2+} and Sr^{2+}, in the range of oxygen activity $-6 < \log a_{O_2} < 0$ at 800°, 900° and 1000°C, respectively. The oxygen self-diffusivity, oxygen defect (interstitial) diffusivity, hole mobility, and partial conductivities in the reversible electrode condition are thereby evaluated against defect concentration, and compared with those of the host $La_2NiO_{4+\delta}$. It has been found that acceptor-doping suppresses the oxygen defect diffusivity by ca. an order of magnitude compared with the undoped host by increasing the migrational enthalpy by 0.3 eV or so. Hole mobility is in the range of 0.15 to 0.20 cm^2/Vs for both the undoped and Ca-doped, and 0.21-0.25 cm^2/Vs for the Sr-doped, with their temperature dependence indicating band conduction. The ionic charge-of-transport, phenomenologically corresponding to the number of holes dragged by an oxygen interstitial upon its transfer, appears to increase with increasing defect concentration and decreasing temperature in the range of 0 to 0.5. The ionic and electronic mobilities depending on the types of dopants are discussed in terms of dopant size.

Keywords: Acceptor-doped $La_2NiO_{4+\delta}$, Onsager matrix, Oxygen diffusivity, Hole mobility, Charge-of-transport, Partial conductivities

Corresponding author, hiyoo@snu.ac.kr

1. Introduction

La_2NiO_4 systems are essentially electronic conductors with a unusually high ionic conductivity, thus, attracting a wide attention as a promising material for IT-SOFC cathodes and oxygen permeation membranes.[1-5] From defect chemical point of view, the host $La_2NiO_{4+\delta}$ is quite unusual in that the majority type disorders are oxygen interstitials O_i'' and holes $h^{\bullet}$, respectively residing in the LaO rock-salt(R) sublayer to mitigate the innate local compressive stress, and in the $LaNiO_3$ perovskite(P) sublayer.[6] Furthermore, these defects deviate not negatively as usual, but unusually positively from the ideal dilute solution behavior.[7,8]

We have been examining the defect structure and mass/charge transport properties of the systems doped with different-size acceptors as well as donors. Recently, we have measured the oxygen excess δ of the systems $La_{1.9}A_{0.1}NiO_{3.95+\delta}$ doped with acceptors $A=Ca^{2+}$ and Sr^{2+}, respectively, and confirmed therefrom the earlier findings[6,7,9-12] that the compressive stress in the R layer enhances the oxygen hyperstoichiometry and the positive deviation of defect behavior is attributed to the hole degeneracy pressure.

The present paper is concerned with the effect of doping different-size acceptors Ca and Sr on the transport properties in comparison with the undoped. For this purpose, we first established the isothermal Onsager transport coefficient matrices for the systems of $La_{1.9}A_{0.1}NiO_{3.95+\delta}$ (A=Ca, Sr) by measuring the chemical diffusivity, the ionic charge-of-transport and the conductivity with ion transfer suppressed, and evaluate therefrom the oxygen self-

diffusivity, the defect diffusivity, the hole mobility, and the partial conductivities in the reversible electrode conditions. We hereby present the results in comparison with the undoped.

2. Measurement Principle

The measurement principle of the Onsager matrix has already been detailed elsewhere[13,14] and hence, will be only excerpted here. For the present systems with oxide ions O^{2-} (denoted by the subscript k=i) and holes h^+ (denoted by k=e) as mobile charged components, all kinds of isothermal transport properties can be condensed into a 2x2 Onsager transport coefficient matrix[14] L coupling the carrier (particle) fluxes J_k and their driving forces, electrochemical potential gradients $\nabla\eta_k$ or

$$\begin{pmatrix} J_i \\ J_e \end{pmatrix} = \begin{pmatrix} L_{ii} & L_{ie} \\ L_{ei} & L_{ee} \end{pmatrix} \begin{pmatrix} -\nabla\eta_i \\ -\nabla\eta_e \end{pmatrix} \tag{1}$$

where $L_{ie}=L_{ei}$ due to Onsager[15,16]. One may then conversely determine the three independent L-coefficients, L_{ii}, L_{ee} and L_{ei} by measuring any three independent properties on the systems. Particularly when a system is essentially electronic or its ionic transference number $t_i\approx0$, and its equation of state with respect to the nonstoichiometry or its thermodynamic factor is known, a simplest choice for these properties may be:[14]

(i) Ionic charge-of-transport, $\alpha_i^* \equiv \frac{L_{ei}}{L_{ii}}$ (2)

(ii) (Electronic) Conductivity with ionic transfer suppressed, $\sigma_e' \equiv F^2 L_{ee}\left(1-\frac{L_{ie}^2}{L_{ii}L_{ee}}\right)$ (3)

(iii) Chemical diffusivity, $\tilde{D}_O = \frac{RTL_{ii}}{2c_i}\left[1-\left(1-\frac{\alpha_i^*}{2}\right)t_i\right]\left(\frac{\partial \log c_i}{\partial \log a_{O_2}}\right)^{-1}$ (4)

Here F, R and T have their usual significance and c_i stands for the concentration of mobile ions, O^{2-}. The last factor on the right-hand-side of Eq. (4) is the thermodynamic factor $f(\theta)$, which may be evaluated from the equation of state with respect to the oxygen nonstoichiometry δ of the system.

These three properties can be easily measured simply by monitoring $\nabla\eta_i$ and $\nabla\eta_e$ upon chemical polarization by passing a constant current under the ion-blocking electrode condition as described in detail elsewhere[14].

3. Experimental

The doped specimens $La_{1.9}Ca_{0.1}NiO_{3.95+\delta}$ and $La_{1.9}Sr_{0.1}NiO_{3.95+\delta}$ were prepared via a wet chemistry route followed by sintering as detailed earlier.[12,17] All the sintered pellets were of single phase and 97±1 % dense with an average grain size of 2.3±0.2 μm. The final compositions were experimentally reconfirmed to be Ca/Ni- and Sr/Ni-ratio of 0.101±0.002 and 0.102±0.002, respectively.[12]

For the measurement of the three properties, α_i^*, σ_e', and $\tilde{D}_O$, by the galvanostatic mode,[14] the electrochemical cell involving the doped specimens (measuring 5.4x4.7x9.6 and 6.2x4.9x10.0 mm^3 for the Ca-doped and Sr-doped, respectively) was constructed into the following configuration,

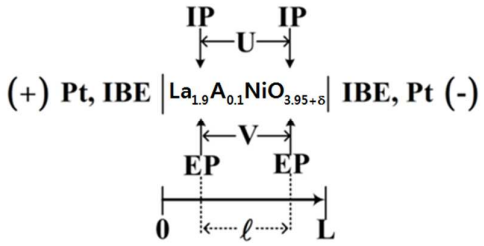

(I)

with a pair of ionic probes (IP) and electronic probes (EP) implanted symmetrically at a distance ℓ (=5.3 and 5.9 mm for A=Ca and Sr, respectively) apart between a pair of ion-blocking electrodes (IBE).

The as-constructed cell is schematically shown in Fig. 1, where the disks of yttria-stabilized zirconia (YSZ, 1 mm thickness) are employed to mechanically block the ionic flux (IBE) when passing a current across the specimen via the electrodes #2 and #7 as well as to measure or monitor, if necessary, the oxygen potentials at the YSZ/specimen interfaces. As the inner ionic (#5 and #6) and electronic probes (#3 and #4), YSZ needles (ca. 100 μm tip radius) and Pt-wires (200 μm diameter) are employed, respectively. The entire cell is embedded in a borosilicate glass for the purpose of hermetic sealing. It has earlier been confirmed[14] that the possible reaction between the $La_2NiO_{4+\delta}$ systems and sealing glass may be neglected.

Before exercising the ion-blocking mode of polarization and depoloarization, the system oxide was first equilibrated by short-circuiting across each of the YSZ disks (IBE), in the surrounding with given oxygen activity a_{O_2}, which was adjusted by N_2/O_2 gas mixtures and monitored by a YSZ oxygen sensor. During polarization by passing a constant dc current I

between the current probes #2 and #7 or depolarization by switching off I, temporal evolution of the electrochemical potential difference of oxide ions $\Delta\eta_i$ between the pair of IPs was monitored by the open-circuit voltage U across them as

$$\nabla \eta_i \approx -\frac{2FU}{\ell} \tag{5}$$

and that of holes $\Delta\eta_e$ by the open-circuit voltage V across the pair of EPs as

$$\nabla \eta_e \approx \frac{FV}{\ell} \tag{6}$$

The applied current (on the level of 80~70 mA) was adjusted to such a level that the resulted U and V never exceeded ~5 mV so that the thermodynamic state of the system may be defined as the oxygen activity a_{O_2} in the surrounding at given temperature T. For the experimental details including the cell construction and measurement, the reader is referred to Ref. 14.

Fig. 1.

4. Results and Discussions

4.1 Onsager L-matrices

Fig. 2 shows the typical temporal variations of U(t) and V(t) upon polarization in one direction (I<0) followed by depolarization (I=0), and consecutive polarization in the opposite direction (I>0) followed by depolarization (I=0) under the ion-blocking condition. No sooner than a constant current I(<0) is switched on, U(t) and V(t) immediately jump up to a specific value, a measure of

the total resistance of the specimen with uniform composition ($\nabla\delta=0$) and then, V(t) saturates almost immediately, characteristic of an electronic conductor ($t_e>>t_i$)[14], but U(t) relaxes towards a non-vanishing finite value, reflecting a diffusion-controlled kinetics. Once the current is switched off at the steady state polarization($t\rightarrow\infty$), V relaxes to 0 almost immediately again because $t_e\approx1$, but U first switches its sign due to the remaining polarization $\Delta\delta(t\rightarrow\infty)$, followed by diffusion-controlled relaxation back to U=0 this time. When polarized in the opposite direction (I>0), the same behavior repeats, but in the opposite sense. It is emphasized that $U(t\rightarrow\infty)$ never vanishes as repeatedly observed,[16,18,19] and it is simply because $L_{ie}\neq0$, see Eq. (1).

Fig. 2

The ionic charge-of-transport, α_i^* and the (electronic) conductivity with ion transfer suppressed, σ_e' are respectively determined by the steady state values U(∞) and V(∞) upon polarization as[14]

$$\alpha_i^* = \frac{2U(\infty)}{V(\infty)} \; ; \quad \sigma_e' = -\frac{I/A}{V(\infty)/\ell} \tag{7}$$

where A stands for the cross sectional area of the specimen (0.25 ± 0.01 cm^2 for the Ca-doped; 0.30 ± 0.01 cm^2 for the Sr-doped).

The chemical diffusivity $\tilde{D}_O$ of the mobile component O, on the other hand, is determined from the temporal variation of U(t)[20] upon polarization as:

$$U(t) = -\frac{\ell I \alpha_i^*}{2A\sigma_e'} - \frac{LIt_e}{A\sigma_e'}\left(1-\frac{\alpha_i^*}{2}\right)\times \\ \frac{4}{\pi^2}\sum_{n=1}^{\infty}\frac{2}{(2n-1)^2}\left(\sin\frac{(2n-1)\pi}{2}\right)\sin\left(\frac{(2n-1)\pi}{2}\frac{\ell}{L}\right)\exp\left(-\frac{\pi^2(2n-1)^2\tilde{D}_O t}{L^2}\right) \tag{8}$$

or upon depolarization therefrom as:

$$U(t) = \frac{LIt_e}{A\sigma_e'}\left(1-\frac{\alpha_i^*}{2}\right)\times \\ \frac{4}{\pi^2}\sum_{n=1}^{\infty}\frac{2}{(2n-1)^2}\sin\left[\frac{(2n-1)\pi}{2}\right]\sin\left[\frac{(2n-1)\pi}{2}\frac{\ell}{L}\right]\exp\left[-\frac{\pi^2(2n-1)^2\tilde{D}t}{L^2}\right] \tag{9}$$

Fitting U(t) to Eq. (8) and (9) additionally results in the numerical values for α_i^* and σ_e', which are, of course, in agreement with those as determined due to Eq. (7) within the experimental errors. The results are all compiled together with their error bounds in Fig. 3.

Fig. 3.

Nonstoichiometry δ (or Δ), as defined as $La_{1.9}A_{0.1}NiO_{3.95+\delta}$ (or $La_{1.9}A_{0.1}NiO_{4.00+\Delta}$), has earlier been documented for the present systems (A=Ca, Sr)[12] as reproduced in Fig. 4(a). By noting that c_i=3.95+δ per molar volume, the thermodynamic factor in Eq. (4) above is subsequently evaluated as

$$f(\theta) = \left(\frac{\partial \log a_{O_2}}{\partial \log c_i}\right) = \left(\frac{3.95+\delta}{\delta}\right)\left(\frac{\partial \log a_{O_2}}{\partial \log \delta}\right), \tag{10}$$

which, after appropriate differentiation of the equation of state given in Ref. 12, takes an analytic form as

$$\left(\frac{\partial \log a_{O_2}}{\partial \log \delta}\right)=\frac{4\beta}{2\beta-[O_I'']}\left(\frac{\partial \log [O_I'']}{\partial \log \delta}\right)+\left[4+\frac{4}{\sqrt{8}}\left(\frac{2\beta\delta}{N_V}\right)+8\left(\frac{3}{16}-\frac{\sqrt{3}}{9}\right)\left(\frac{2\beta\delta}{N_V}\right)^2\right] \quad (11)$$

with

$$\left(\frac{\partial \log [O_I'']}{\partial \log \delta}\right)=\frac{\beta\delta}{2[O_I'']}\left\{1-\frac{2K_F+(K_F-1)(\delta-x/2)}{\left[(6K_F+(K_F-1)(\delta-x/2))^2-8K_F(K_F-1)(4+(\delta-x/2))\right]^{1/2}}\right\} \quad (12)$$

Here, β is the numerical factor ($=N_A/V_m$, N_A being the Avogadro number and V_m the molar volume), $[O_I'']$ the concentration of O_I'' (in number/unit volume), x the site fraction of A(=Ca, Sr) (=0.10 in the present cases), N_V the effective density of states at valence band, and K_F the Frenkel equilibrium constant. The thermodynamic factors calculated as such are shown in Fig. 4(b).

Fig. 4.

Finally, by solving simultaneously Eqs. (2), (3) and (4) in association with $f(\theta)$ in Eq. (10), one can evaluate the three independent Onsager coefficients for the present systems as shown in Fig. 5. It is seen that L_{ee} is more than 4 orders of magnitude larger than L_{ii}, confirming $t_e >> t_i$, and L_{ie} is only a few factors smaller than L_{ii}, confirming the ion-electron interference effect not to be negligible at all as repeatedly observed.[16,18,19,21,22]

Fig. 5.

4.2 Oxygen self-diffusivity and defect diffusivity

L_{ii} is a direct measure of the self-diffusivity D_O of mobile component O[‡], viz.,

$$L_{ii} = \frac{D_O c_O}{RT} \tag{13}$$

Here, c_O is the concentration of component O, which takes a value

$$c_O = \frac{3.95 + \delta}{V_m} = \frac{4.00 + \Delta}{V_m}, \tag{14}$$

depending on whether the nonstoichiometry is defined relative to the electronic stoichiometric composition ($La_{1.90}A_{0.10}NiO_{3.95+\delta}$) or ionic stoichiometric composition ($La_{1.90}A_{0.10}NiO_{4.00+\Delta}$). The as-calculated self-diffusivities of O for A=Ca and Sr are shown in comparison with that of the undoped host in Fig. 6.

Fig. 6.

As has been expected from the defect structure of undoped and acceptor-doped systems,[7,12] the self-diffusivity increases with increasing oxygen activity in agreement with the concomitant concentration change of the majority ionic disorders, O_i''. Fig. 7 compares the as-evaluated self-

[‡] The present systems have the tetragonal structure. If they were all single crystals, their diffusion coefficients should, thus, be anisotropic with two principal values. The present specimens, however, are polycrystalline with no texture and hence, may be regarded as isotropic with the single diffusivity value as confirmed by the fitted results of U(t) to Eq. (8) or (9) (solid lines in Fig. 2).

diffusivities in air atmosphere with the tracer diffusivities reported in literatures.[1,3,23] As is seen, the former are in general agreement with the latter.

Fig. 7.

In the range of oxygen activity examined in the present study, the oxygen vacancy concentration may be neglected compared to that of oxygen interstitials. We can, thus, evaluate the defect diffusivity of O_I'', D_I due to the relationship,

$$D_O = D_I \frac{\Delta}{4 + \Delta} \quad (15).$$

We plot the as-evaluated D_O in Fig. 6 against the fraction of O_I'', $\Delta/(4+\Delta)$[§] in Fig. 8. It is noted that they are highly linearly correlated no matter whether doped or undoped, indicating that the defect diffusivity is independent of defect concentration, as has been the case. From the slopes, the interstitial defect diffusivities are evaluated against temperature as shown in Fig. 9. They are each best represented as:

[§] Here, the interstitials are defined as the excess over the ionic stoichiometric composition $\Delta=0$.

(i) Undoped, $$D_I / cm^2 s^{-1} = \left(8.8^{+7.5}_{-4.0}\right) \times 10^{-3} \exp\left(-\frac{0.64 \pm 0.06}{kT}\right) \quad (16a)$$

(ii) Ca-doped, $$D_I / cm^2 s^{-1} = \left(1.6^{+1.8}_{-1.3}\right) \times 10^{-2} \exp\left(-\frac{0.90 \pm 0.02}{kT}\right) \quad (16b)$$

(iii) Sr-doped, $$D_I / cm^2 s^{-1} = \left(1.9^{+2.2}_{-1.7}\right) \times 10^{-2} \exp\left(-\frac{0.97 \pm 0.02}{kT}\right) \quad (16c)$$

Fig. 8.

Fig. 9.

One can see that the ionic defect diffusivity or mobility is suppressed by acceptor doping by ca. an order of magnitude compared to the undoped. The activation energies in Eq. (16) should correspond to the enthalpy ΔH_m for O_I'' migration through the R-layer, which are ca. 0.3 eV larger for the acceptor-doped than the undoped.[18] The physico-chemical origin of the larger ΔH_m and hence, smaller D_I for the acceptor-doped is yet to be elucidated. We suspect that the possible reduction of free-volume of the R-layer due to acceptor-doping may be the culprit. To check this suspicion, we have tried to estimate the free-volume, $V_{Free,R}$ of the R-layer. It is known[24] that the unit cell volumes of these systems, whether doped or not, are nearly independent of oxygen activity or oxygen content, though the lattice constant "a" and "c" are, of course, separately dependent on it. By using the refinement of XRD results as measured in air in

the earlier study,[12] thus, we have first calculated the total volume of an LaO R-layer as $V_{tot,R}$= $a^2 \cdot h$ where h is the height of an R-layer in a tetragonal unit cell, and subtracted therefrom the volume occupied by the host and guest ions in the R-layer on the basis of Shannon's compilation.[25] Looking at Fig. 10, one can see that ΔH_m decreases with increasing $V_{Free,R}$ as such. In the absence of evidence to the contrary, we may, thus, say that ΔH_m -increase and concomitant D_I-suppression with acceptor-doping is attributed not to the stress at the interface between the R- and P-layers in the La_2NiO_4 structure, but to the $V_{Free,R}$ –reduction due to doping.

Fig. 10.

4.3 Hole Mobility

What L_{ee} is to electronic carriers** is what L_{ii} is to ionic carriers:

$$L_{ee} = \frac{D_h}{RT} c_h = \frac{u_h}{F} \frac{\delta}{V_m} \tag{17}$$

in the present oxygen activity range where holes ($h^{\bullet}$) are in the majority. Here, u_h denotes the electrochemical mobility of holes as $\alpha_e^* \to 0$ or at infinite dilution ($\delta \to 0$). It is noted that $c_h=\delta/V_m$ whereas $c_I=\Delta/V_m$.

In order to determine the mobility on the basis of Eq. (17), we plot L_{ee} for the three

** If single crystal, then L_{ee} should also be anisotropic, but here assumed to be isotropic because the specimens are polycrystalline with no texture, see the footnote for Eq. (13).

systems against δ at different temperatures in Fig. 11. One can see that L_{ee} vs. δ are all highly linearly correlated, clearly indicating that u_h is independent of hole concentration for all the systems at all temperatures. The mobilities have been evaluated from the slopes as listed in Table 1, where the literature values for the undoped[2,7,26] are also given for comparison purpose. For the undoped case, it takes a value of 0.15-0.19 cm^2/Vs in agreement with the reported within the experimental error. Compared to the undoped, the hole mobility appears to have been increased by acceptor-doping, the most by Sr-doping and less by Ca-doping, but the latter case is not so unambiguous considering the error bounds. A general trend, nevertheless, appears to be the decrease of the mobility with temperature, indicating a band conduction in agreement with the earlier study on the undoped.[7,26] Any trend of change with the dopants here should be attributed to the difference in dopant size because the dopants have the same valence of +2. We have thus probed any systematic correlation between the mobility and the size effect. When doped with different-sized dopants, one can immediately consider the possible distortion of the P-layer in which electronic conduction occurs. Again using the refinement of XRD results, we have calculated the tolerance factor of the P-layer as a measure of its distortion and examined the correlation to the hole mobility. The results are as shown in Fig. 12. The mobility reduces with increasing tolerance factor over 1, even if the mobility datum of the undoped at 900°C is off the trend. We here conjecture that Ni d-orbitals are rendered less overlapped as the tolerance factor increases, thus, the hole mobility decreases.

Table 1.

Fig. 11.

Fig. 12.

4.4. Ionic Charge of Transport

The ionic charge of transport α_i^* is a measure of the interference effect between ionic carriers O_I'' and electronic carriers $h^{\bullet}$ upon their transfer. Phenomenologically this corresponds to the number of $h^{\bullet}$ dragged by an O_I'' in the reversible electrode condition, thus, one may take -2+ α_i^* to be the effective charge of O_I'' upon its transfer.[27] Translation of the Onsager-Fuoss-Debye-Hückel theory on the cross effect in electrolytic solutions into the mixed ionic electronic condution[28] suggests that α_i^* should increase with increasing ionic strength or defect concentration and decreasing temperature due to diminishing thermal disordering effect. We hereby re-plot the charge of transport α_i^* vs. $\log a_{O_2}$ in Fig. 3(a) into α_i^* vs. log Δ in Fig. 13 with the aid of the equation of state with respect to oxygen excess.[7,12,18] It appears that α_i^* increases with Δ and decreasing T, but only in qualitative agreement with the theory.[28] Clearly, we need to collect more data on the charge-of-transport in more systematic way for a quantitative

understanding of the cross effect. What is certain, nevertheless, is that the interference effect is by no means negligible and even appreciable depending on defect concentration, contrary to the old wisdom, e.g., Kohlausch's law of independent migration of charge carriers and Nernst-Einstein equation connecting the self-diffusivity and conductivity.[27]

Fig. 13.

4.5. Partial ionic and electronic conductivities

When $\alpha_i^* \neq 0$, one should distinguish the partial ionic conductivity in the reversible electrode condition, σ_i from the conductivity with electronic transfer suppressed in the electron-blocking condition, σ_i'.[27,29]

$$\sigma_i = 4F^2 L_{ii}\left(1 - \frac{L_{ie}}{2L_{ii}}\right) \; ; \quad \sigma_i' = 4F^2 L_{ii}\left(1 - \frac{L_{ie}^2}{L_{ii}L_{ee}}\right) \tag{18}$$

Likewise for electronic conductivities,

$$\sigma_e = F^2 L_{ee}\left(1 - \frac{2L_{ie}}{L_{ee}}\right) \; ; \quad \sigma_e' = F^2 L_{ee}\left(1 - \frac{L_{ie}^2}{L_{ii}L_{ee}}\right) \tag{19}$$

One can recognize that $\sigma_i = \sigma_i'$ and $\sigma_e = \sigma_e'$ only when $L_{ie}=0$. For the documentation purpose, we here calculate the partial conductivities σ_i and σ_e, and compile against oxygen activity in Fig. 14 in comparison with those of the undoped host.

Fig. 14.

Summary and Conclusions

By measuring the three different transport properties, α_i^*, σ_e and $\tilde{D}_O$ in association with the thermodynamic factor, we have established the 2x2 Onsager transport coefficient matrices against oxygen activity ($-6 < \log a_{O_2} < 0$) and temperature (1073≤T/K≤1273) for the acceptor-doped La_2NiO_4, systems, $La_{1.9}Ca_{0.1}NiO_{3.95+\delta}$ and $La_{1.9}Sr_{0.1}NiO_{3.95+\delta}$. We have thereby evaluated the oxygen self-diffusivity, oxygen interstitial-diffusivity, hole mobility and partial electronic and ionic conductivities. It is found that the ionic mobility is suppressed by ca. an order of magnitude by acceptor doping compared to the undoped host, which is ascribed to the reduction of the free volume for interstitial migration in the LaO rock-salt sublayers. Hole mobility, on the other hand, appears to be enhanced by the acceptor doping, which is ascribed to the reduction of the tolerance factor of the $LaNiO_3$ perovskite sublayers compared with the undoped host. It is further found that the law of independent migration of ionic and electronic carriers clearly breaks down and hence, the effective charge of oxygen interstitials goes from -2 up to -1.6 as defect concentration increases and temperature decreases.

Acknowledgements

This work was financially supported by the POSCO Distinguished Professor Program through RIST funded by POSCO, Korea.

References

[1] J. M. Bassat, P. Odier, A. Villesuzanne, C. Marin and M. Pouchard, *Solid State Ionics*, 2004, **167**, 341-347.

[2] A. L. Shaula, E. N. Naumovich, A. P. Viskup, V. V. Pankov, A. V. Kovalevsky and V. V. Kharton, *Solid State Ionics*, 2009, **180**, 812-816.

[3] J. A. Kilner and C. K. M. Shaw, *Solid State Ionics*, 2002, **154-155**, 523-527.

[4] L. Minervini, R. W. Grimes, J. A. Kilner and K. E. Sickafus, *J. Mater. Chem.*, 2000, **10**, 2349-2354.

[5] A. Tarancon, M. Burriel, J. Santiso, S. J. Skinner and J. A. Kilner, *J. Mater. Chem.*, 2010, **20**, 3799-3813.

[6] J. Wan, J.B. Goodenough, and J.H. Zhu, *Solid State Ionics*, 2007, **178**, 281-286.

[7] H.-S. Kim and H.-I. Yoo, *Phys. Chem. Chem. Phys.*, 2010, **12**, 4704-4713.

[8] H.-S. Kim and H.-I. Yoo, *Solid State Ionics*, 2012, **229**, 59-73.

[9] T. Nakamura, K. Yashiro, K. Sato, and J. Mizusaki, *J. Solid State Chem.*, 2009, **182**, 1533-1537.

[10] P. Odier, Ch. Allançon, and J. M. Bassat, *J. Solid State Chem.*, 2000, **153**, 381-385.

[11] M. Yashima, N. Sirikanda and T. Ishihara, *J. Am. Chem. Soc.*, 2010, **132**, 2385-2392.

[12] H.-S. Kim and H.-I. Yoo, *Solid State Ionics*, 2013, **232**, 129-137.

[13] H.-I. Yoo and H.-S. Kim, *Solid State Ionics*, 2013, **225**, 166-171.

[14] H.-S. Kim and H.-I. Yoo, *Phys. Chem. Chem. Phys.*, 2010, **12**, 12951-12955.

[15] L. Onsager, *Phys. Rev.*, 1931, **37**, 405 ; 1931, **38**, 2265-2279.

[16] D.-K. Lee and H.-I. Yoo, *Phys. Rev. Lett.*, 2006, **97**, 255901/1-4.

[17] D.-P. Huang, Q. Xu, W. Chen, F. Zhang and H.–X. Liu, *Ceram. Int.*, 2008, **34**, 651-655.

[18] H.-S. Kim and H.-I. Yoo, *Phys. Chem. Chem. Phys.*, 2011, **13**, 4651-4658.

[19] C. Chatzichristodoulou, W.-S. Park, H.-S. Kim, P. V. Hendriksen, and H.-I. Yoo, *Phys. Chem. Chem. Phys.*, 2010, **12,** 9637-9649.

[20] K.-C. Lee and H.-I. Yoo, *J. Phys. Chem. Solids*, 1999, **60**, 911-927.

[21] H.-I. Yoo and J.-H. Lee, *Solid State Ionics*, 1995, **80**, 5-9.

[22] J.-O. Hong and H.-I. Yoo, *Solid State Ionics*, 1998, **113-115**, 265-270.

[23] S. J. Skinner and J. A. Kilner, *Solid State Ionics*, 2000, **135**, 709-712.

[24] T. Nakamura, K. Yashiro, K. Sato and J. Mizusaki, *Solid State Ionics*, 2010, **181** 292-299.

[25] R. D. Shannon, *Acta Cryst.*, 1976, **A32**, 751-767.

[26] T. Nakamura, K. Yashiro, K. Sato, and J. Mizusaki, *Phys. Chem. Chem. Phys.*, 2009, **11**, 3055-3062.

[27] H.-I. Yoo and J.-H. Lee, *J. Phys. Chem. Solids*, 1996, **57[1]**, 65-73.

[28] J. Janek, M. Martin and H.-I. Yoo, *Ber. Busenges. Phys. Chem.*, 1994, **98[5]**, 655-664.

[29] C. Wagner, *Prog. Solid State Chem.*, 1975, **10**, 3-16.

Table Caption

Table 1. Hole mobility, u_h of $La_{1.9}Ca_{0.1}NiO_{3.95+\delta}$, $La_{1.9}Sr_{0.1}NiO_{3.95+\delta}$ and $La_2NiO_{4+\delta}$ at different temperatures, in comparison with the literature values[2,7,26] available.

Figure Captions

Fig. 1. Schematic of the as-constructed polarization cell. 1 & 8, reversible gas electrodes; 2 & 7, Pt current probes; 3 & 4, Pt-electronic probes; 5 & 6, YSZ-ionic probes.

Fig. 2. Typical temporal variations of U and V of $La_{1.9}Ca_{0.1}NiO_{3.95+\delta}$ upon switching on a constant current in one direction (I=-80 mA), off the current (I=0), on in the opposite direction (I=+80mA,) and finally off the current (I=0) again at 900 °C and $\log a_{O_2}$ =-2.07. The solid lines through the U-data are the best fitted to Eqs. (8) and (9) in the text. Note that U does go to a non-vanishing, finite value as $t\rightarrow\infty$ upon polarization.

Fig. 3. The ionic charge-of-transport (a), conductivity with ionic transfer suppressed (b), and chemical diffusivity (c) vs. oxygen activity at different temperatures for $La_{1.90}Ca_{0.10}NiO_{3.95+\delta}$ (top) and $La_{1.9}Sr_{0.1}NiO_{3.95+\delta}$ (bottom). Dashed lines are only for visual guidance.

Fig. 4. Oxygen nonstoichiometry δ (a) and thermodynamic factor (b) vs. oxygen activity at different temperatures for A=Ca (top) and Sr(bottom) of $La_{1.9}A_{0.1}NiO_{3.95+\delta}$. Data in (a), reproduced from Ref. 12.

Fig. 5. The Onsager coefficients L_{ii}, L_{ee} and L_{ie}(=L_{ei}) vs. oxygen activity of $La_{1.9}A_{0.1}NiO_{3.95+\delta}$ for

A=Ca(a) and Sr(b) at different temperatures.

Fig. 6. Oxygen self-diffusivities vs. oxygen activity of $La_{1.9}A_{0.1}NiO_{3.95+\delta}$ (A=Ca and Sr) in comparison with that of undoped $La_2NiO_{4+\delta}$[18] at 800°C(a), 900°C(b) and 1000°C(c). Dashed lines are for visual guidance only.

Fig. 7. Comparison of the oxygen self-diffusivities of undoped $La_2NiO_{4+\delta}$ and acceptor-doped $La_{1.9}A_{0.1}NiO_{3.95+\delta}$ with the literature data on O^{18}-tracer diffusivity.[1,3,23]

Fig. 8. D_O vs. $\Delta/(4+\Delta)$ of $La_2NiO_{4+\delta}$ ($\delta=\Delta$), $La_{1.9}Ca_{0.1}NiO_{3.95+\delta}$($\delta=\Delta+0.05$), and $La_{1.9}Sr_{0.1}NiO_{3.95+\delta}$($\delta=\Delta+0.05$) at 800°C(a), 900°C(b) and 1000°C(c).

Fig. 9. Oxygen interstitial diffusivity vs. reciprocal temperature of $La_2NiO_{4+\delta}$, $La_{1.9}Ca_{0.1}NiO_{3.95+\delta}$, and $La_{1.9}Sr_{0.1}NiO_{3.95+\delta}$. Solid lines are the best-fitted linearly.

Fig. 10. Correlation between the activation enthalpy for migration of O_I'' and the free volume available to the interstitials in the LaO-layer of $La_{1.9}A_{0.1}NiO_{3.95+\delta}$. Dashed line is only for visual guidance.

Fig. 11. L_{ee} vs. δ of undoped and two acceptor-doped La_2NiO_4 systems at 800°C (a), 900°C (b) and 1000°C (c).

Fig. 12. Hole mobility vs. tolerance factor of the P-layer of undoped La_2NiO_4 and acceptor-doped $La_{1.9}A_{0.1}NiO_{3.95+\delta}$ with A=Ca and Sr at different temperatures. Dashed lines are only for visual guidance.

Fig. 13. Ionic charge of transport vs. oxygen interstitial concentration Δ, in semilogarithmic scale, of the undoped and two acceptor-doped La_2NiO_4 at 800°C(a), 900°C(b) and 1000°C(c).

Fig. 14. Partial ionic and electronic conductivities vs. oxygen activity for the undoped and the two acceptor doped La_2NiO_4 at 800°C(a), 900°C(b) and 1000°C(c). Dashed lines are only for visual guidance.

Table 1

Temp./°C	u_h/cm²V⁻¹s⁻¹		
	Undoped	Ca-doped	Sr-doped
800	0.18 ± 0.01 0.22 [2], 0.17 [7], 0.24 [26]	0.20 ± 0.01	0.25 ± 0.02
900	0.19 ± 0.01 0.21 [2], 0.16 [7], 0.22 [26]	0.18 ± 0.01	0.23 ± 0.02
1000	0.15 ± 0.01 0.14 [7]	0.17 ± 0.01	0.21 ± 0.02

Fig. 1

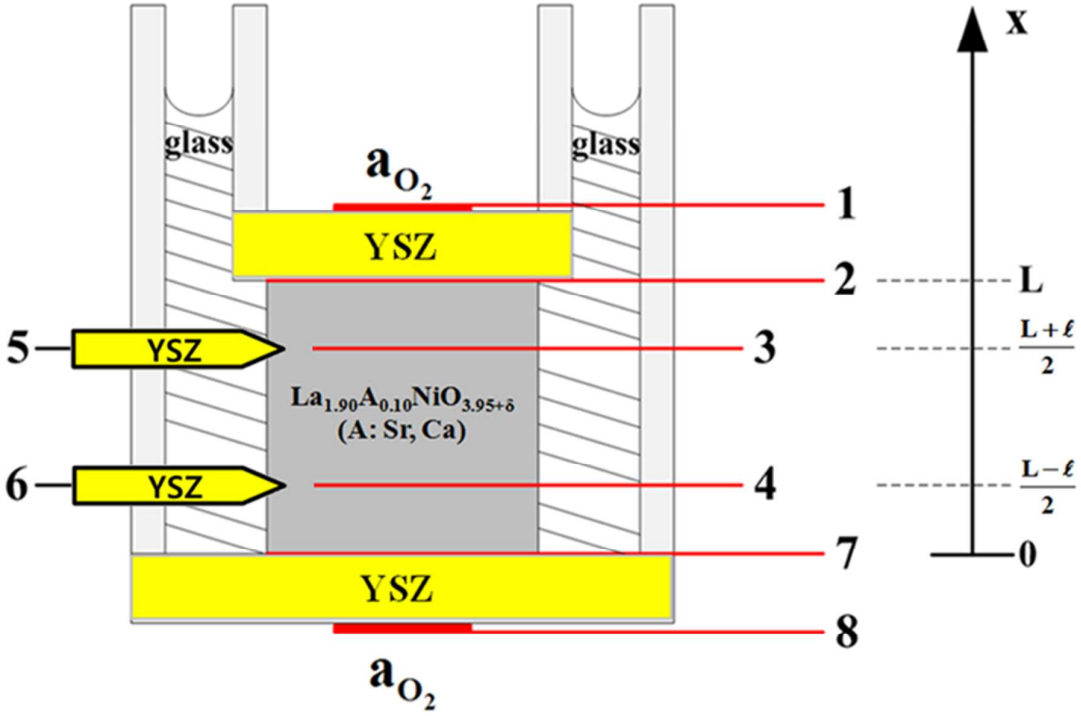
glass
glass
a_{O_2}
YSZ
$La_{1.90}A_{0.10}NiO_{3.95+\delta}$
(A: Sr, Ca)
YSZ
YSZ
YSZ
a_{O_2}
1
2
3
4
5
6
7
8
x
L
$\frac{L+\ell}{2}$
$\frac{L-\ell}{2}$
0

Fig. 2

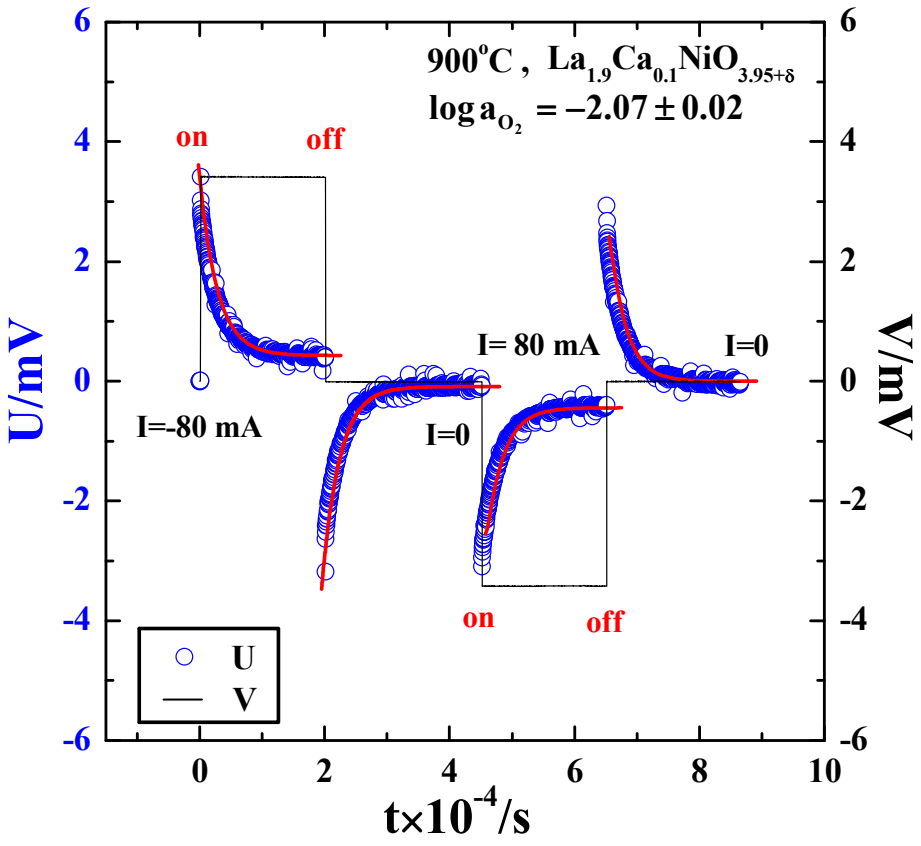
900°C , La1.9Ca0.1NiO3.95+δ
log aO2 = −2.07 ± 0.02
on
off
I=-80 mA
I= 80 mA
I=0
I=0
on
off
U
V
U/mV
V/mV
t×10-4/s
6
4
2
0
-2
-4
-6
0
2
4
6
8
10

Fig. 3

(a)

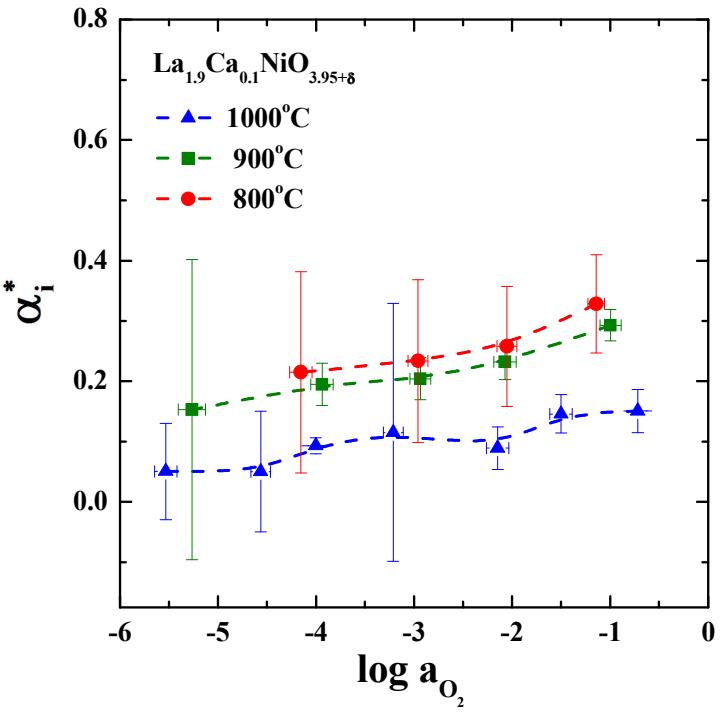
La1.9Ca0.1NiO3.95+δ
1000°C
900°C
800°C
α*i
log aO2
0.8
0.6
0.4
0.2
0.0
-6
-5
-4
-3
-2
-1
0

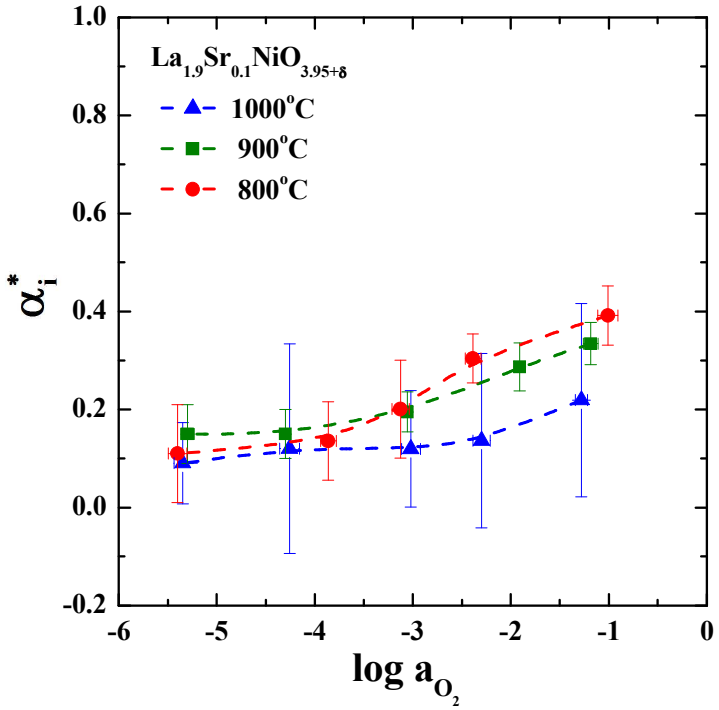
La1.9Sr0.1NiO3.95+δ
1000°C
900°C
800°C
α*i
log aO2
1.0
0.8
0.6
0.4
0.2
0.0
-0.2
-6
-5
-4
-3
-2
-1
0

(b)

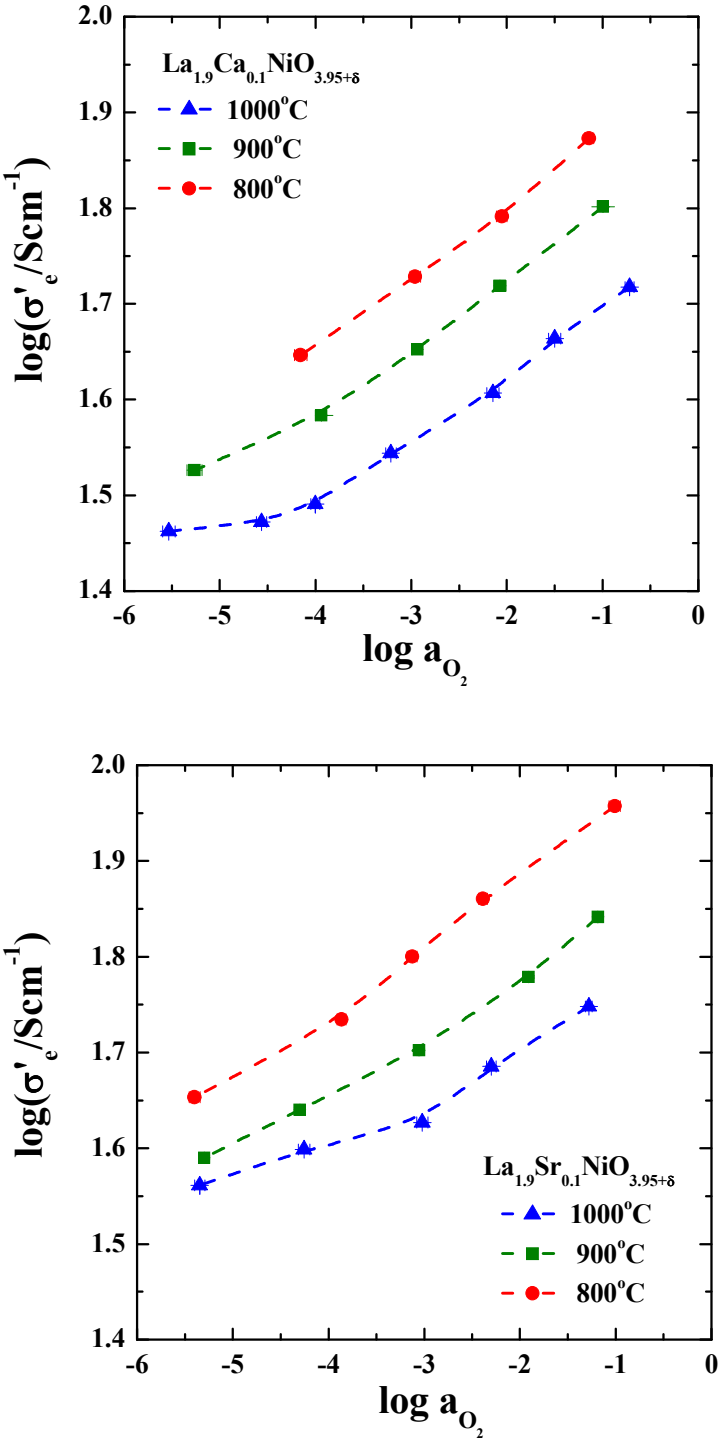
La1.9Ca0.1NiO3.95+δ
1000°C
900°C
800°C
log(σ'e/Scm-1)
log aO2
La1.9Sr0.1NiO3.95+δ
1000°C
900°C
800°C
log(σ'e/Scm-1)
log aO2

(c)

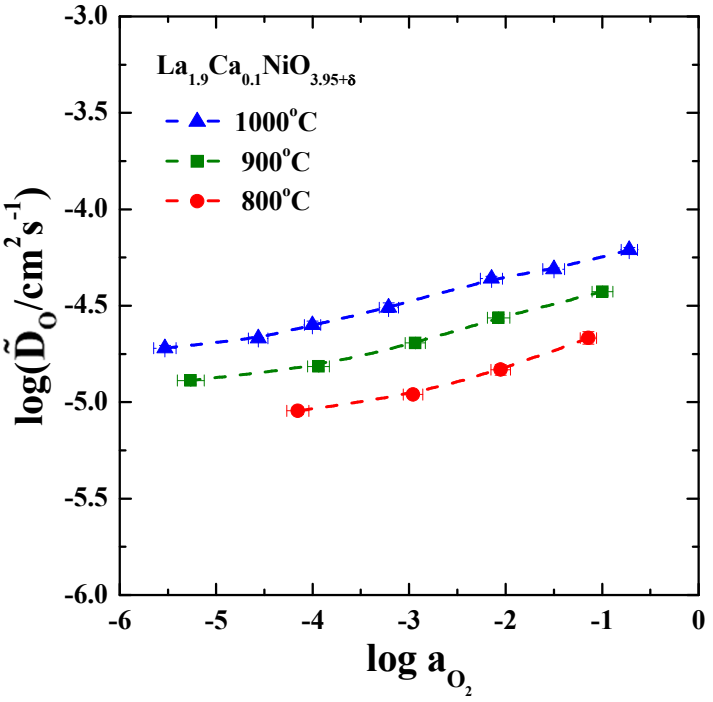
La1.9Ca0.1NiO3.95+δ
1000°C
900°C
800°C
log(D̃O/cm2s-1)
log aO2
-3.0
-3.5
-4.0
-4.5
-5.0
-5.5
-6.0
-6
-5
-4
-3
-2
-1
0

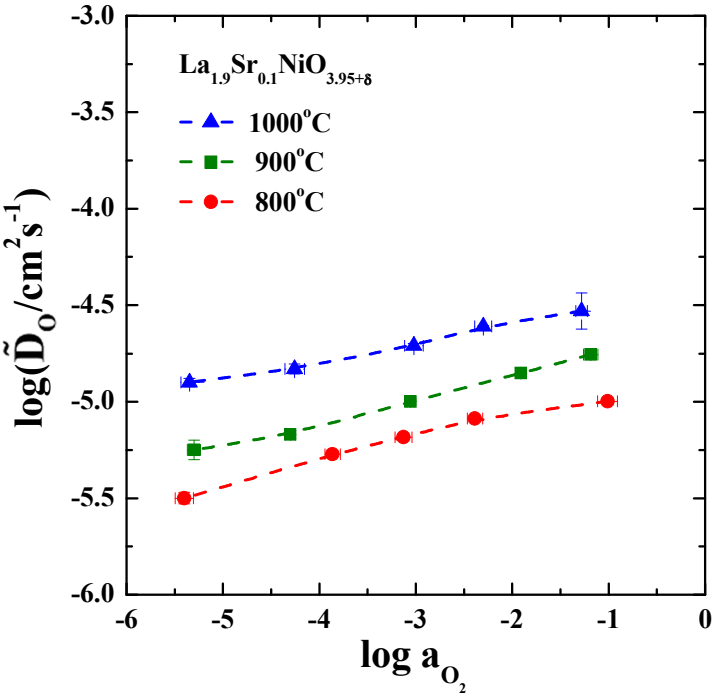
La1.9Sr0.1NiO3.95+δ
1000°C
900°C
800°C
log(D̃O/cm2s-1)
log aO2
-3.0
-3.5
-4.0
-4.5
-5.0
-5.5
-6.0
-6
-5
-4
-3
-2
-1
0

Fig. 4

(a)

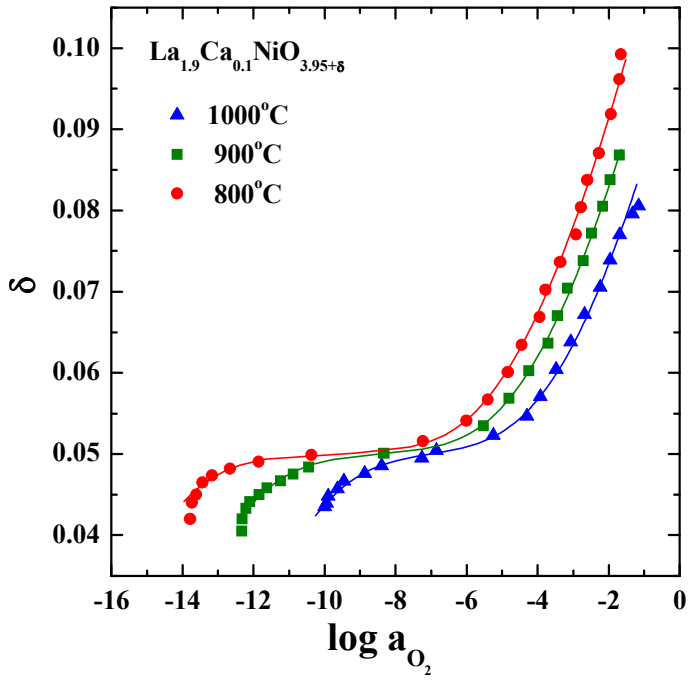
La1.9Ca0.1NiO3.95+δ
1000°C
900°C
800°C
δ
log a O2
0.10
0.09
0.08
0.07
0.06
0.05
0.04
-16
-14
-12
-10
-8
-6
-4
-2
0

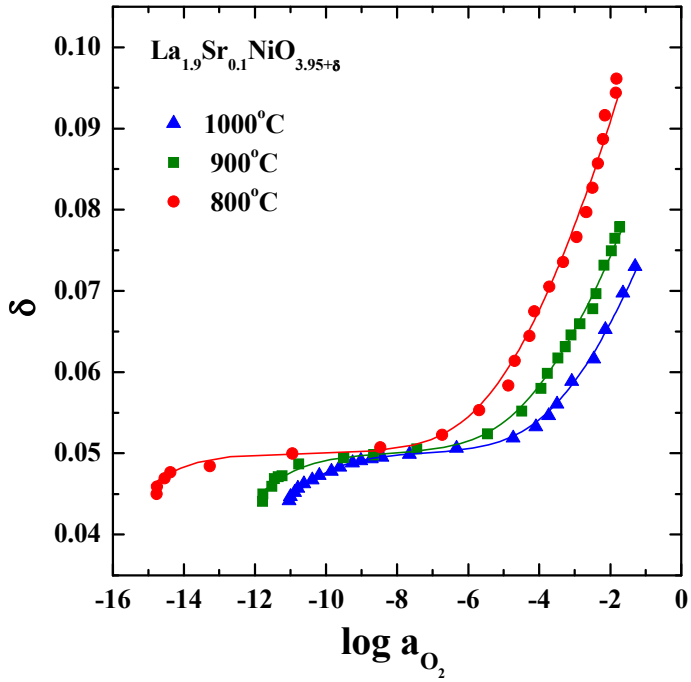
La1.9Sr0.1NiO3.95+δ
1000°C
900°C
800°C
δ
log a O2
0.10
0.09
0.08
0.07
0.06
0.05
0.04
-16
-14
-12
-10
-8
-6
-4
-2
0

Fig. 4

(b)

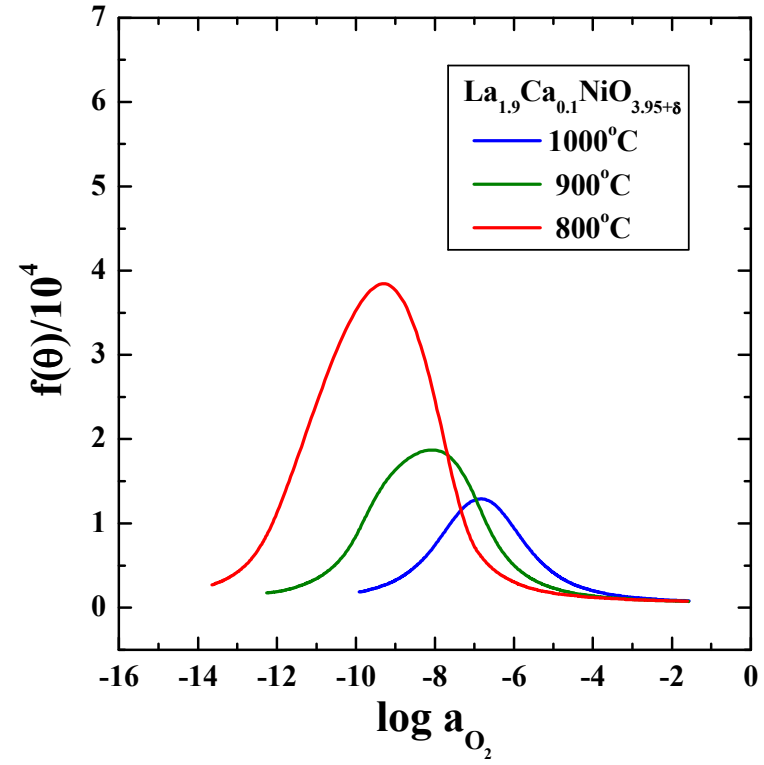
La1.9Ca0.1NiO3.95+δ
1000°C
900°C
800°C
f(θ)/10^4
log a_O2
7
6
5
4
3
2
1
0
-16
-14
-12
-10
-8
-6
-4
-2
0

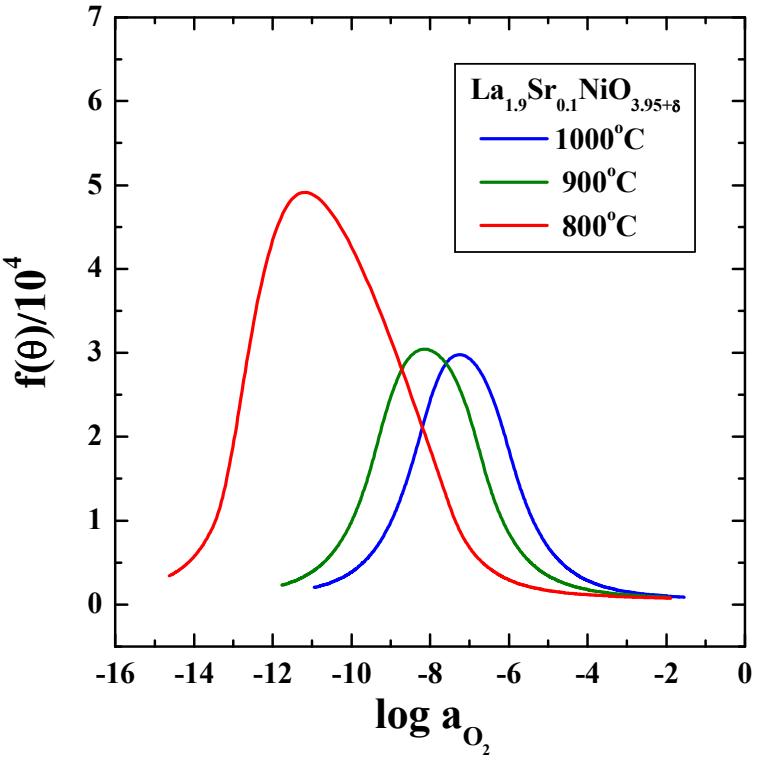
La1.9Sr0.1NiO3.95+δ
1000°C
900°C
800°C
f(θ)/10^4
log a_O2
7
6
5
4
3
2
1
0
-16
-14
-12
-10
-8
-6
-4
-2
0

Fig. 5

(a)

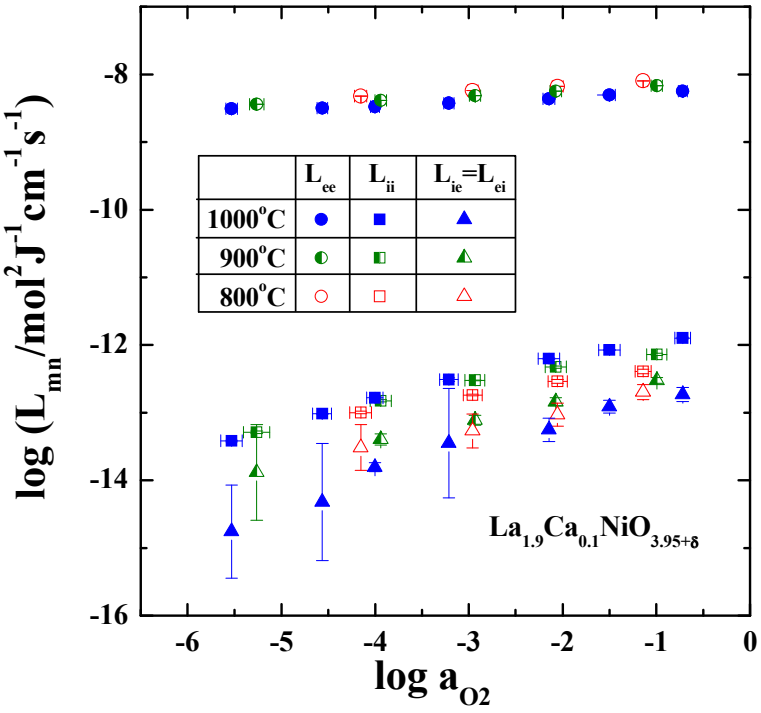
log (L_mn /mol²J⁻¹cm⁻¹s⁻¹)
log a_O2
L_ee
L_ii
L_ie=L_ei
1000°C
900°C
800°C
La1.9Ca0.1NiO3.95+δ

(b)

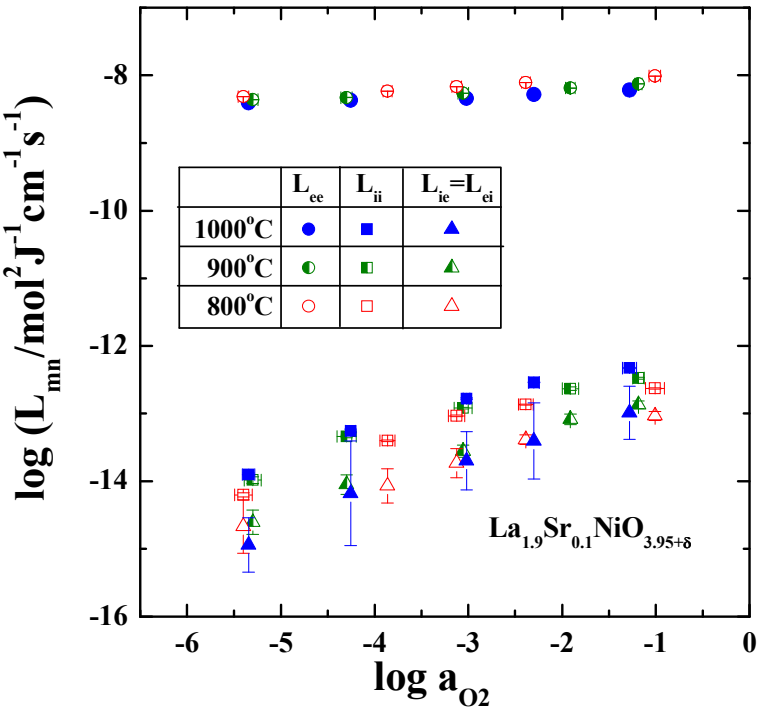
log (L_mn /mol²J⁻¹cm⁻¹s⁻¹)
log a_O2
L_ee
L_ii
L_ie=L_ei
1000°C
900°C
800°C
La1.9Sr0.1NiO3.95+δ

Fig. 6

(a)

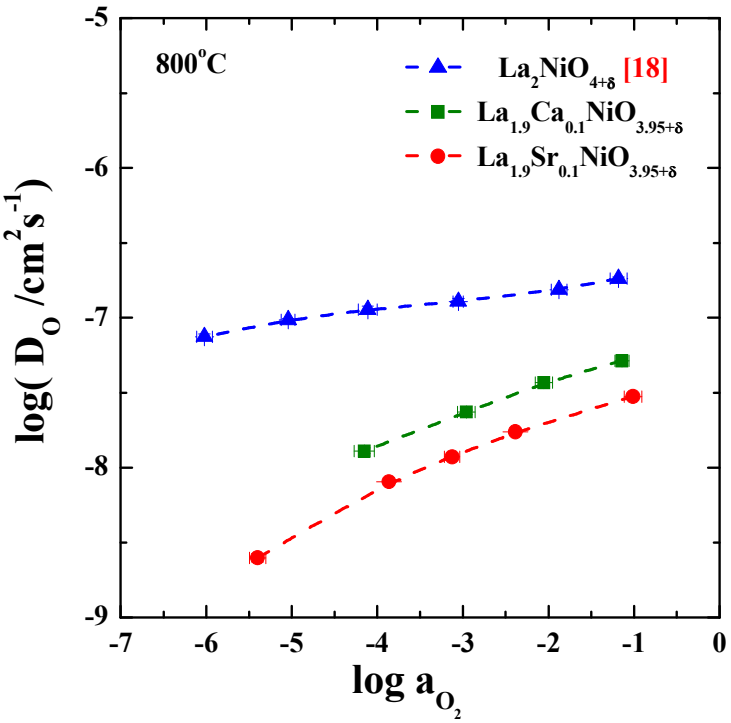
800°C
La2NiO4+δ [18]
La1.9Ca0.1NiO3.95+δ
La1.9Sr0.1NiO3.95+δ
log(DO /cm2 s-1)
log aO2
-5
-6
-7
-8
-9
-7
-6
-5
-4
-3
-2
-1
0

(b)

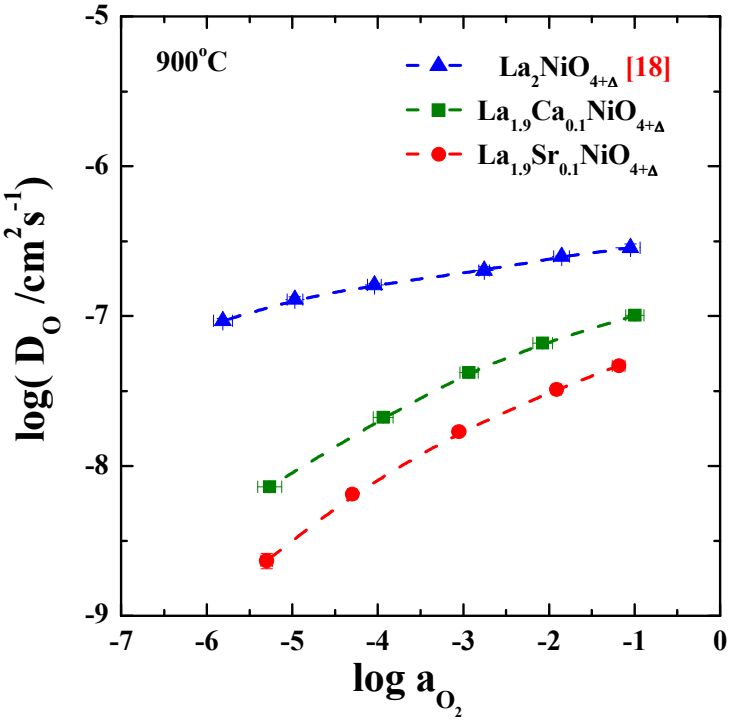
900°C
La2NiO4+Δ [18]
La1.9Ca0.1NiO4+Δ
La1.9Sr0.1NiO4+Δ
log(DO /cm2 s-1)
log aO2
-5
-6
-7
-8
-9
-7
-6
-5
-4
-3
-2
-1
0

(c)

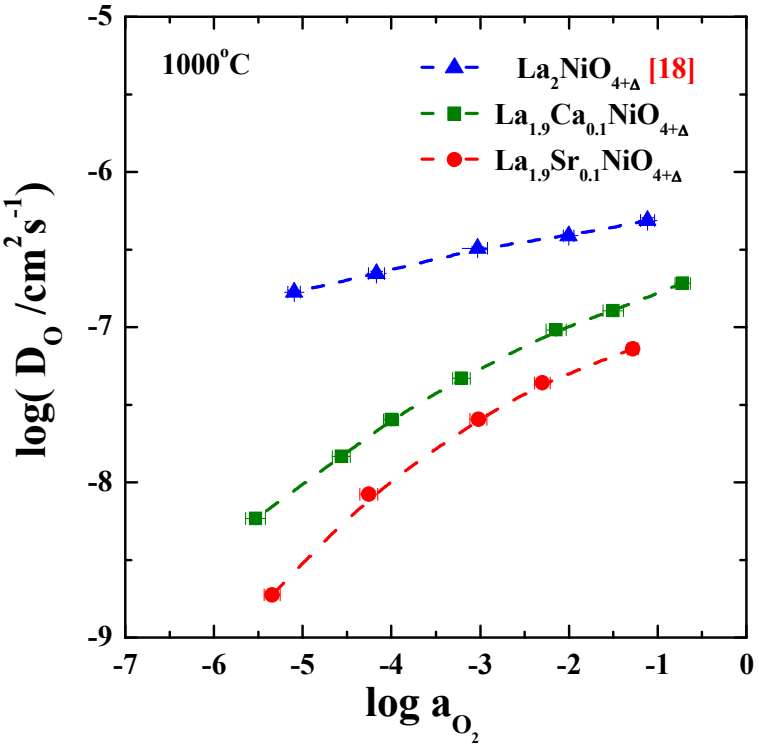
1000°C
La2NiO4+Δ [18]
La1.9Ca0.1NiO4+Δ
La1.9Sr0.1NiO4+Δ
log(DO /cm2s-1)
log aO2
-5
-6
-7
-8
-9
-7
-6
-5
-4
-3
-2
-1
0

Fig. 7

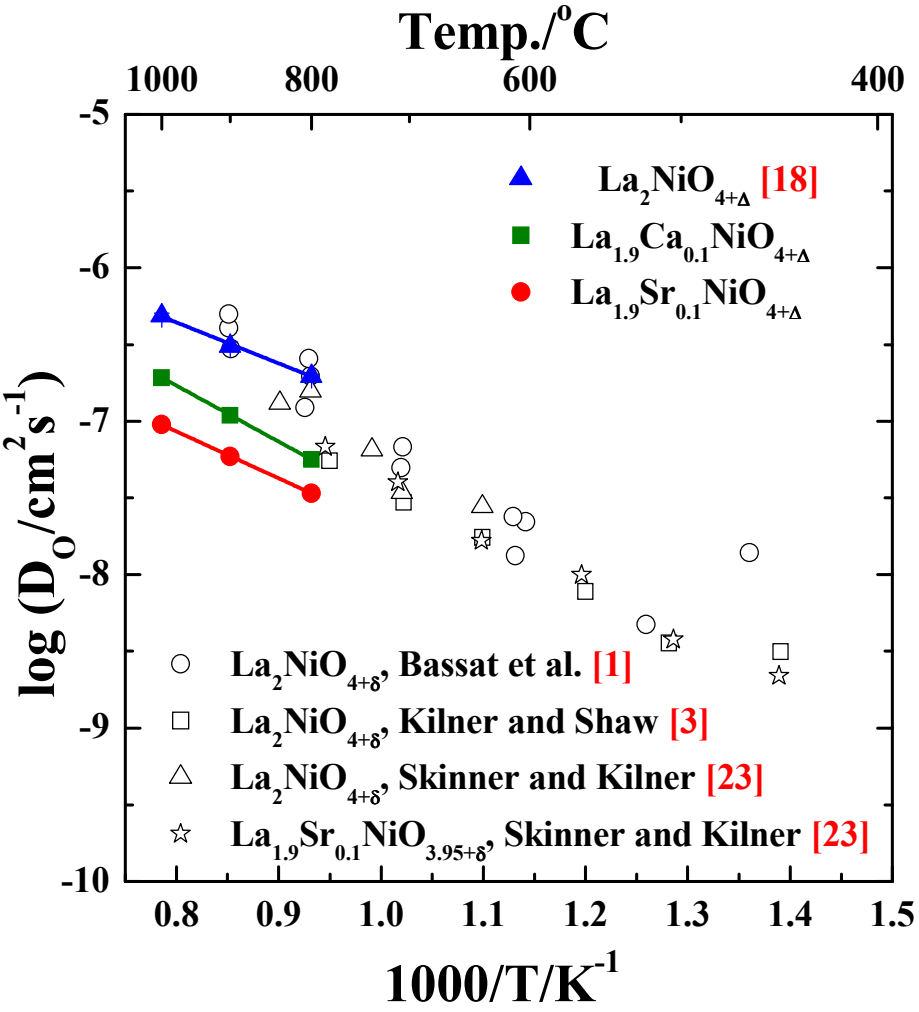
Temp./°C
1000
800
600
400
-5
-6
-7
-8
-9
-10
log (D_O/cm^2 s^-1)
La2NiO4+Δ [18]
La1.9Ca0.1NiO4+Δ
La1.9Sr0.1NiO4+Δ
La2NiO4+δ, Bassat et al. [1]
La2NiO4+δ, Kilner and Shaw [3]
La2NiO4+δ, Skinner and Kilner [23]
La1.9Sr0.1NiO3.95+δ, Skinner and Kilner [23]
0.8
0.9
1.0
1.1
1.2
1.3
1.4
1.5
1000/T/K^-1

Fig. 8

(a)

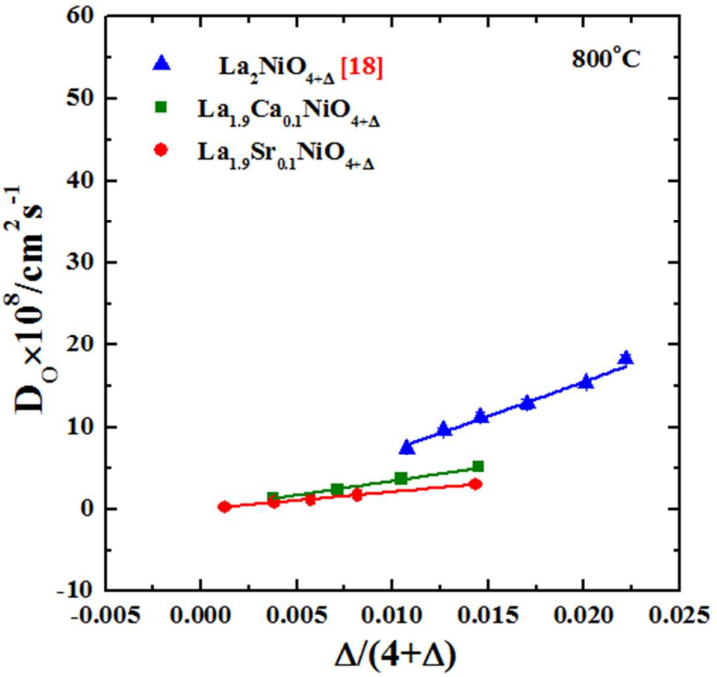
800°C
La2NiO4+Δ [18]
La1.9Ca0.1NiO4+Δ
La1.9Sr0.1NiO4+Δ
DO×10^8/cm^2 s^-1
Δ/(4+Δ)
60
50
40
30
20
10
0
-10
-0.005
0.000
0.005
0.010
0.015
0.020
0.025

(b)

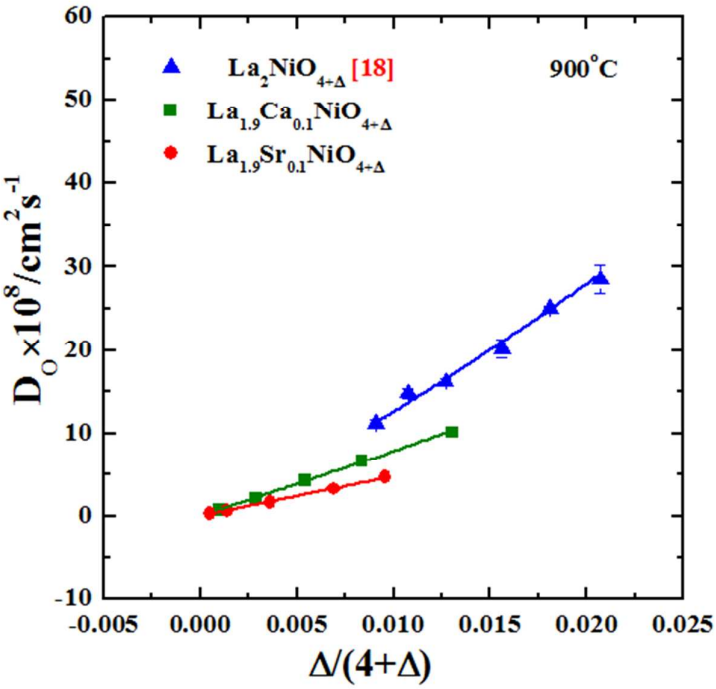
900°C
La2NiO4+Δ [18]
La1.9Ca0.1NiO4+Δ
La1.9Sr0.1NiO4+Δ
DO×10^8/cm^2 s^-1
Δ/(4+Δ)
60
50
40
30
20
10
0
-10
-0.005
0.000
0.005
0.010
0.015
0.020
0.025

(c)

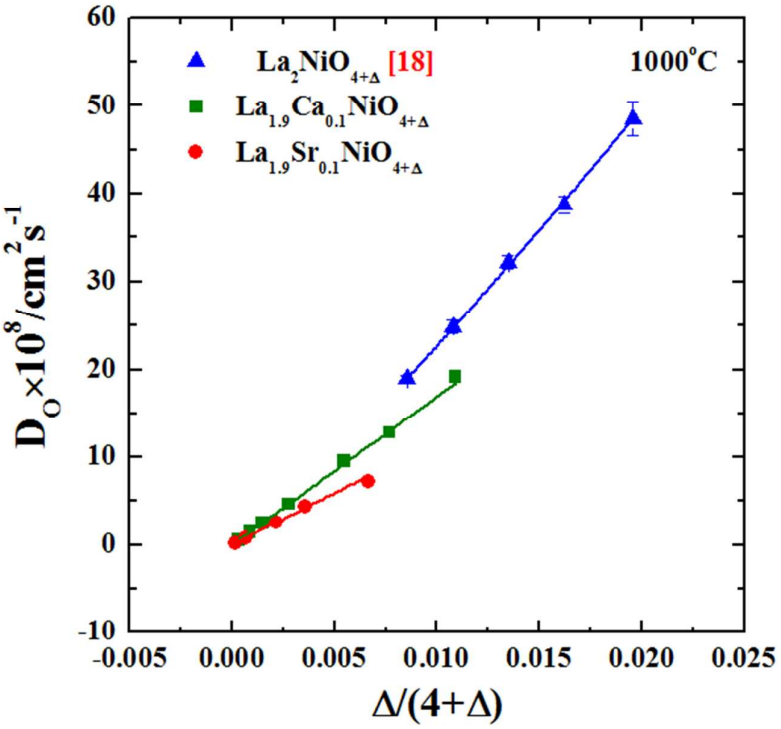
La2NiO4+Δ [18]
1000°C
La1.9Ca0.1NiO4+Δ
La1.9Sr0.1NiO4+Δ
DO×10^8/cm^2 s^-1
Δ/(4+Δ)
60
50
40
30
20
10
0
-10
-0.005
0.000
0.005
0.010
0.015
0.020
0.025

Fig. 9

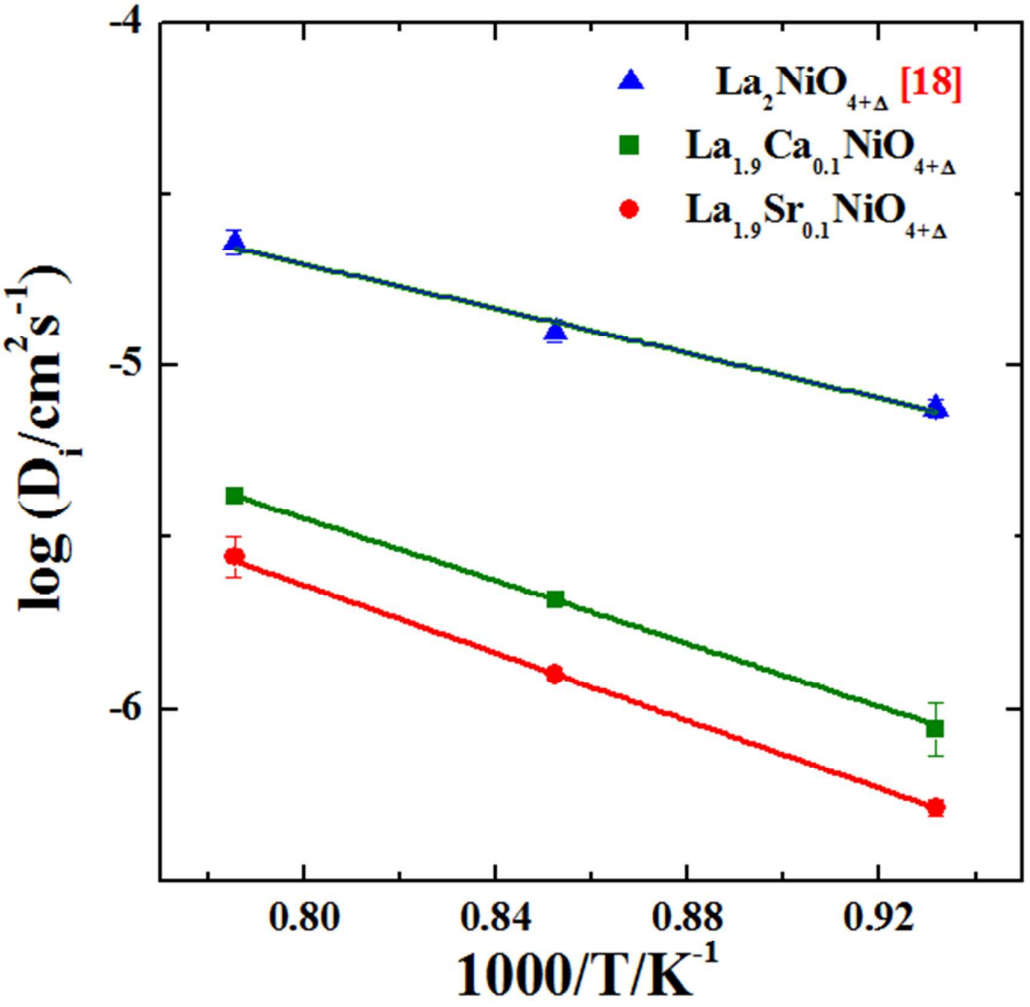
-4
-5
-6
log (D_i/cm^2 s^-1)
La2NiO4+Δ [18]
La1.9Ca0.1NiO4+Δ
La1.9Sr0.1NiO4+Δ
0.80
0.84
0.88
0.92
1000/T/K^-1

Fig. 10

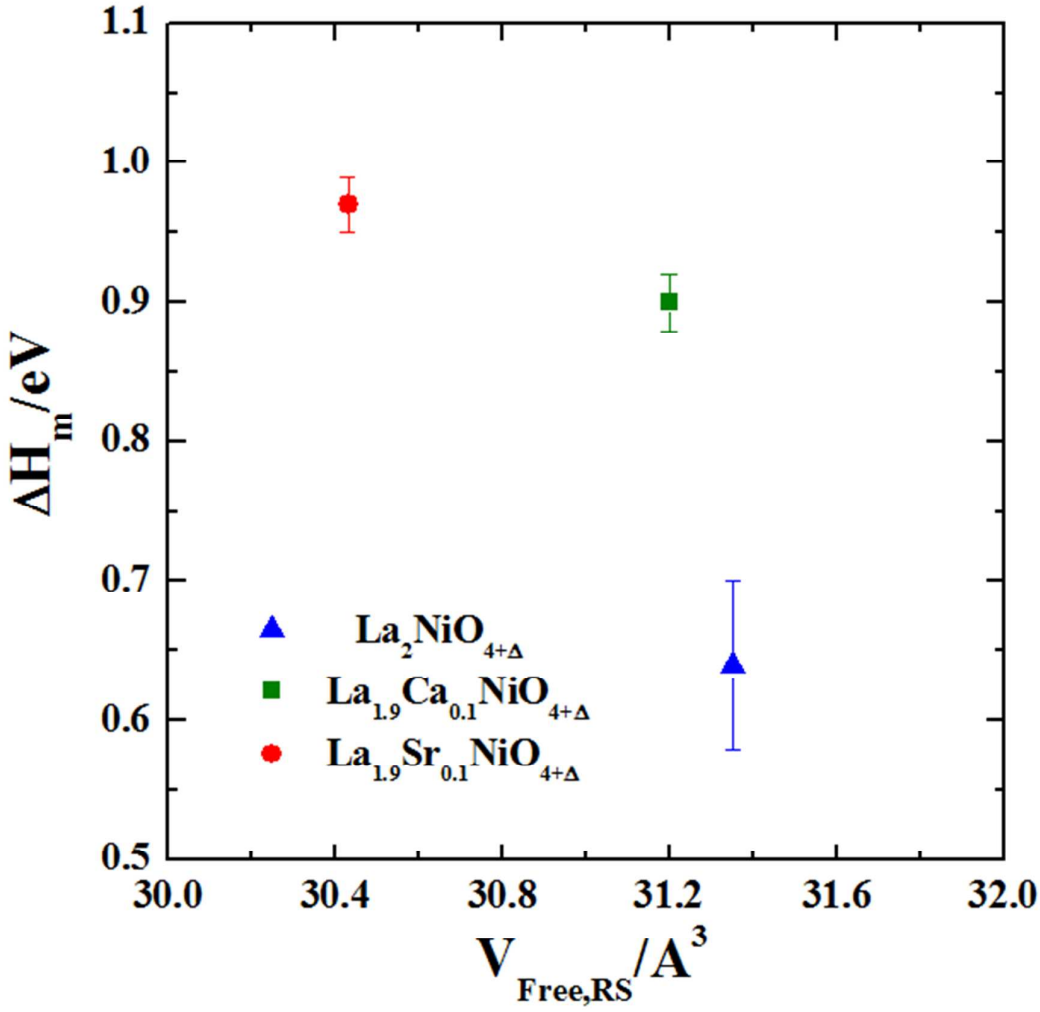
1.1
1.0
0.9
0.8
0.7
0.6
0.5
ΔH_m /eV
30.0
30.4
30.8
31.2
31.6
32.0
V_Free,RS /A^3
La2NiO4+Δ
La1.9Ca0.1NiO4+Δ
La1.9Sr0.1NiO4+Δ

Fig. 11

(a)

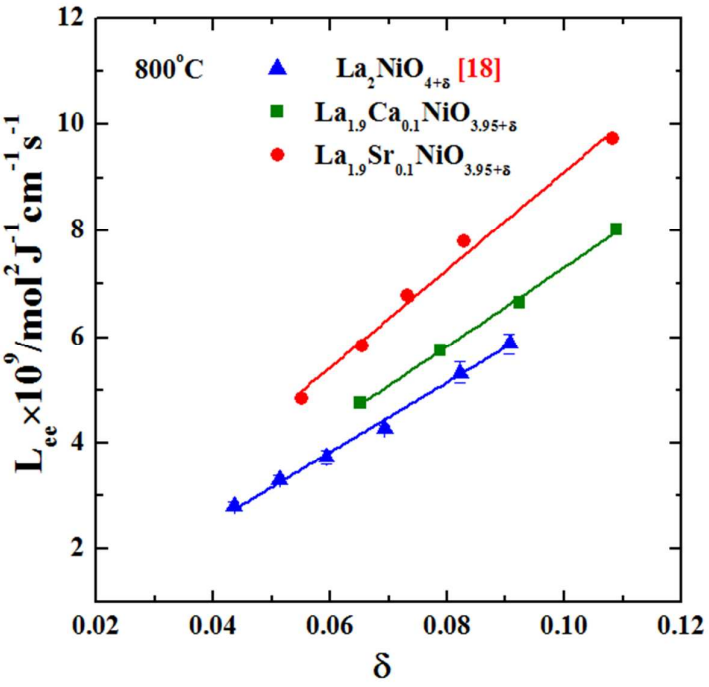
800°C
La2NiO4+δ [18]
La1.9Ca0.1NiO3.95+δ
La1.9Sr0.1NiO3.95+δ
Lee×10^9/mol^2J^-1cm^-1s^-1
δ
12
10
8
6
4
2
0.02
0.04
0.06
0.08
0.10
0.12

(b)

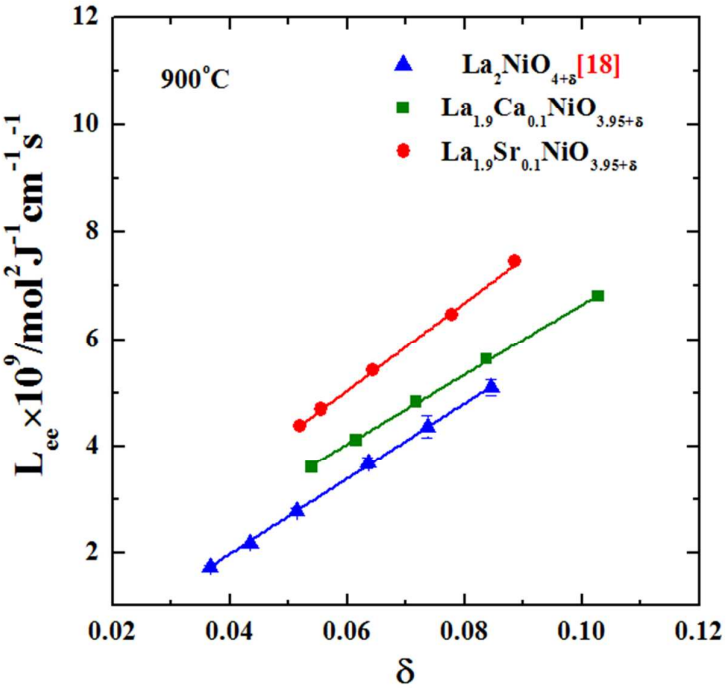
900°C
La2NiO4+δ[18]
La1.9Ca0.1NiO3.95+δ
La1.9Sr0.1NiO3.95+δ
Lee×10^9/mol^2J^-1cm^-1s^-1
δ
12
10
8
6
4
2
0.02
0.04
0.06
0.08
0.10
0.12

(c)

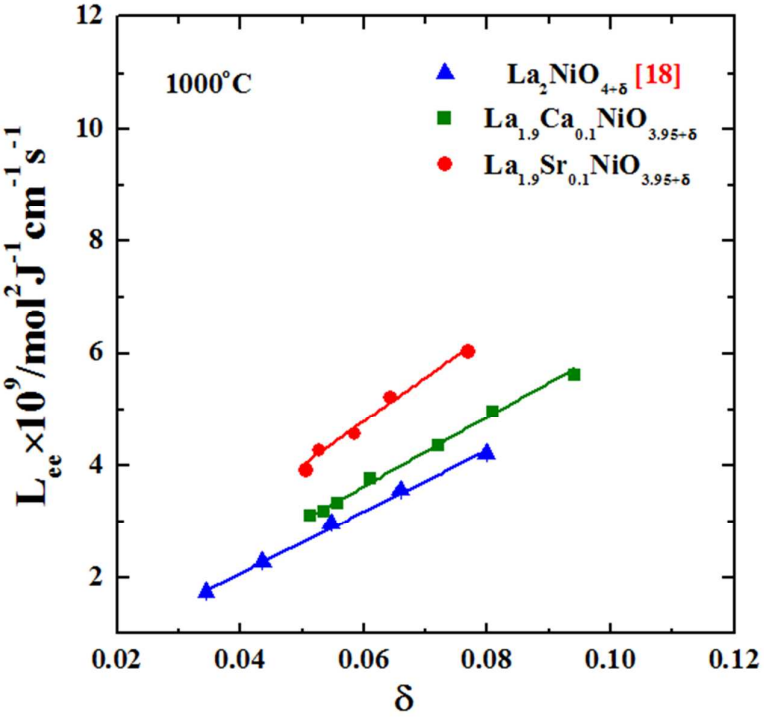
1000°C
La2NiO4+δ [18]
La1.9Ca0.1NiO3.95+δ
La1.9Sr0.1NiO3.95+δ
Lee ×10^9/mol^2J^-1cm^-1 s^-1
δ
12
10
8
6
4
2
0.02
0.04
0.06
0.08
0.10
0.12

Fig. 12

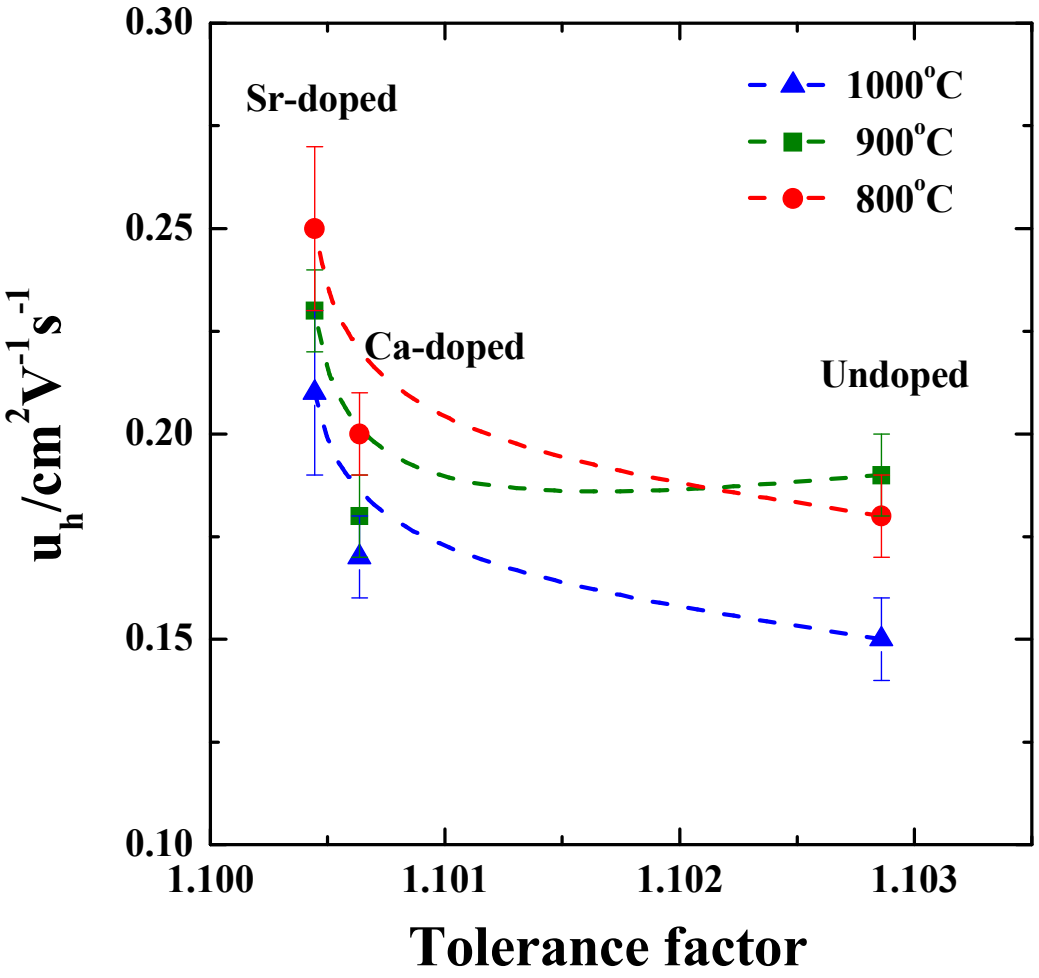
0.30
0.25
0.20
0.15
0.10
1.100
1.101
1.102
1.103
Tolerance factor
u_h/cm^{2}V^{-1}s^{-1}
Sr-doped
Ca-doped
Undoped
1000°C
900°C
800°C

Fig. 13

(a)

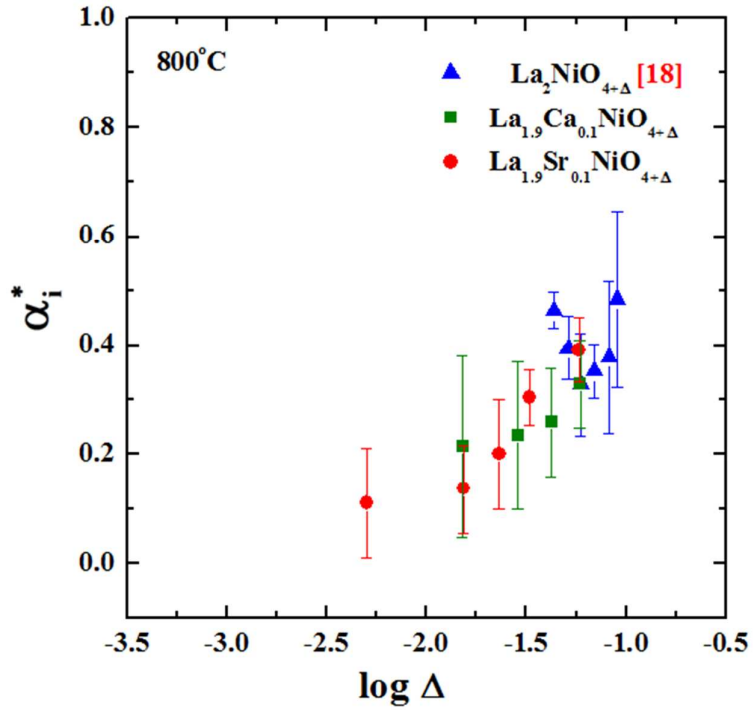
800°C
La2NiO4+Δ [18]
La1.9Ca0.1NiO4+Δ
La1.9Sr0.1NiO4+Δ
α*i
log Δ
1.0
0.8
0.6
0.4
0.2
0.0
-3.5
-3.0
-2.5
-2.0
-1.5
-1.0
-0.5

(b)

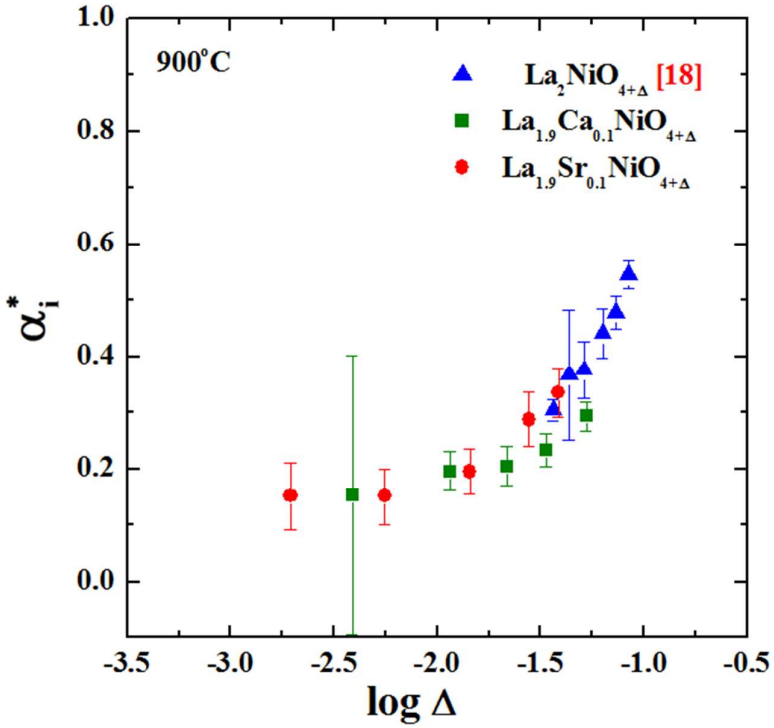
900°C
La2NiO4+Δ [18]
La1.9Ca0.1NiO4+Δ
La1.9Sr0.1NiO4+Δ
α*i
log Δ
1.0
0.8
0.6
0.4
0.2
0.0
-3.5
-3.0
-2.5
-2.0
-1.5
-1.0
-0.5

(c)

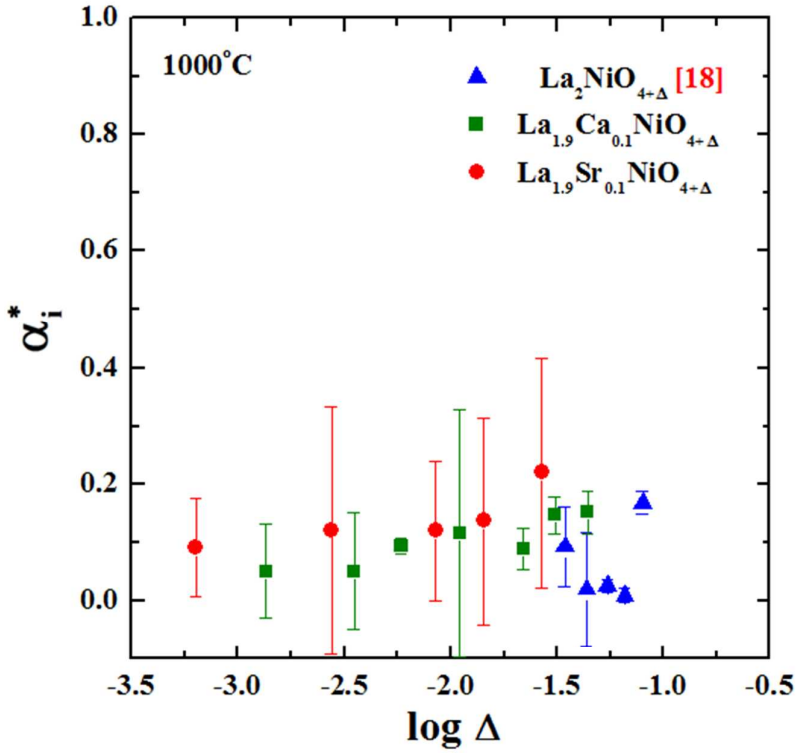
1000°C
La2NiO4+Δ [18]
La1.9Ca0.1NiO4+Δ
La1.9Sr0.1NiO4+Δ
α*i
log Δ
1.0
0.8
0.6
0.4
0.2
0.0
-3.5
-3.0
-2.5
-2.0
-1.5
-1.0
-0.5

Fig. 14

(a)

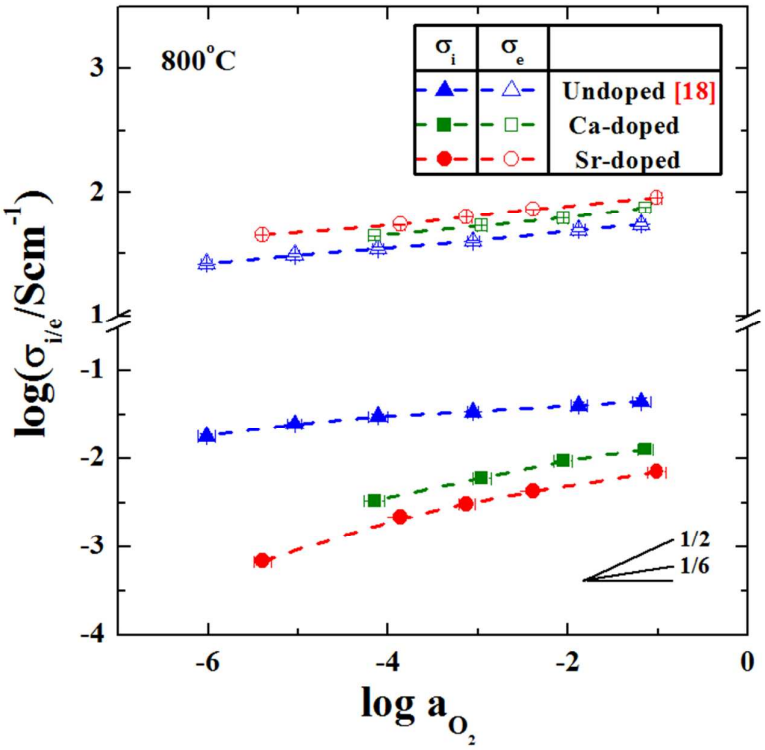
800°C
σi
σe
Undoped [18]
Ca-doped
Sr-doped
1/2
1/6
log(σi/e/Scm-1)
log aO2
3
2
1
-1
-2
-3
-4
-6
-4
-2
0

(b)

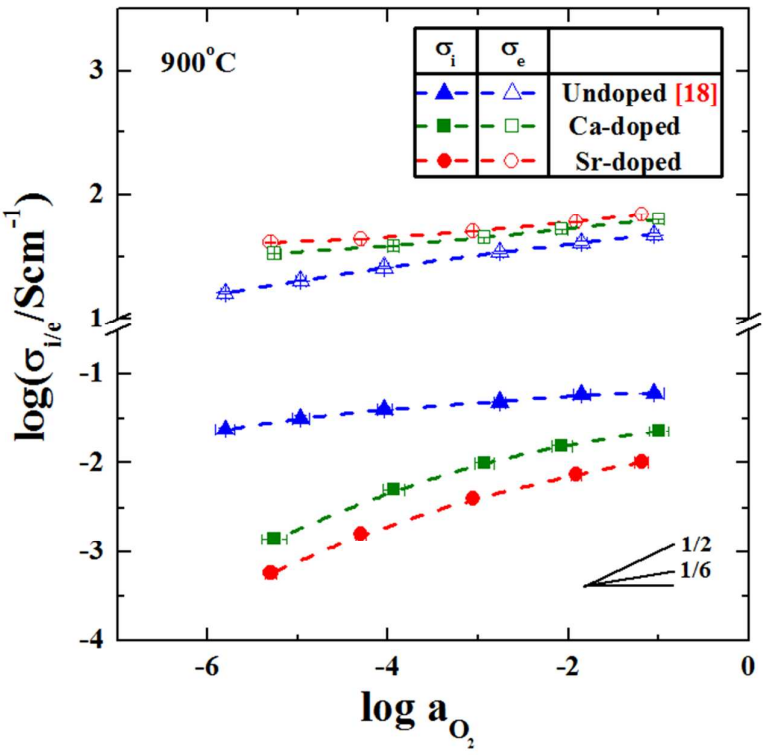
900°C
σi
σe
Undoped [18]
Ca-doped
Sr-doped
1/2
1/6
log(σi/e/Scm-1)
log aO2
3
2
1
-1
-2
-3
-4
-6
-4
-2
0

(c)

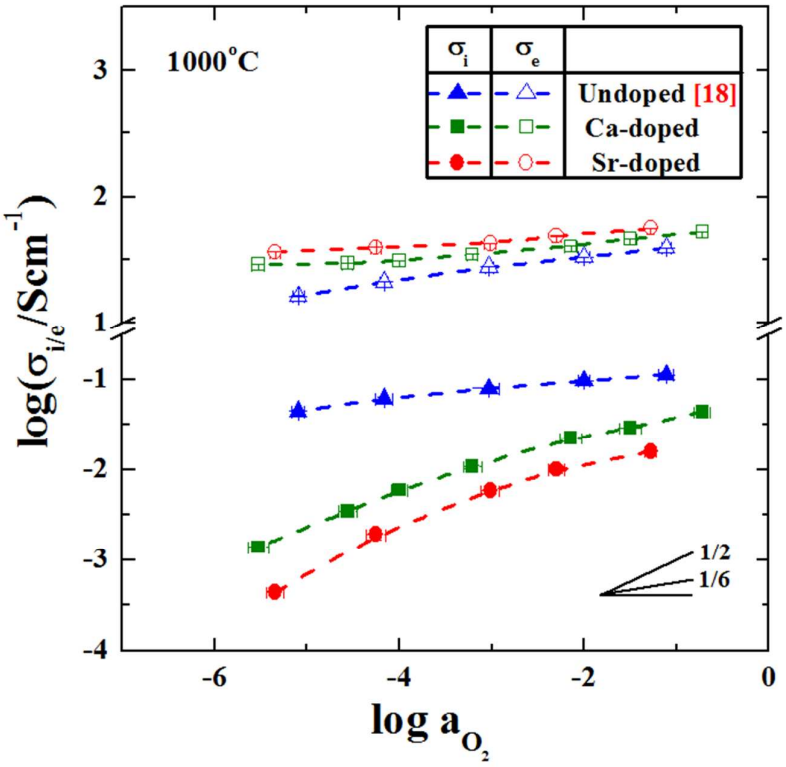
1000°C
σi
σe
Undoped [18]
Ca-doped
Sr-doped
1/2
1/6
log(σi/e/Scm-1)
log aO2
3
2
1
-1
-2
-3
-4
-6
-4
-2
0